

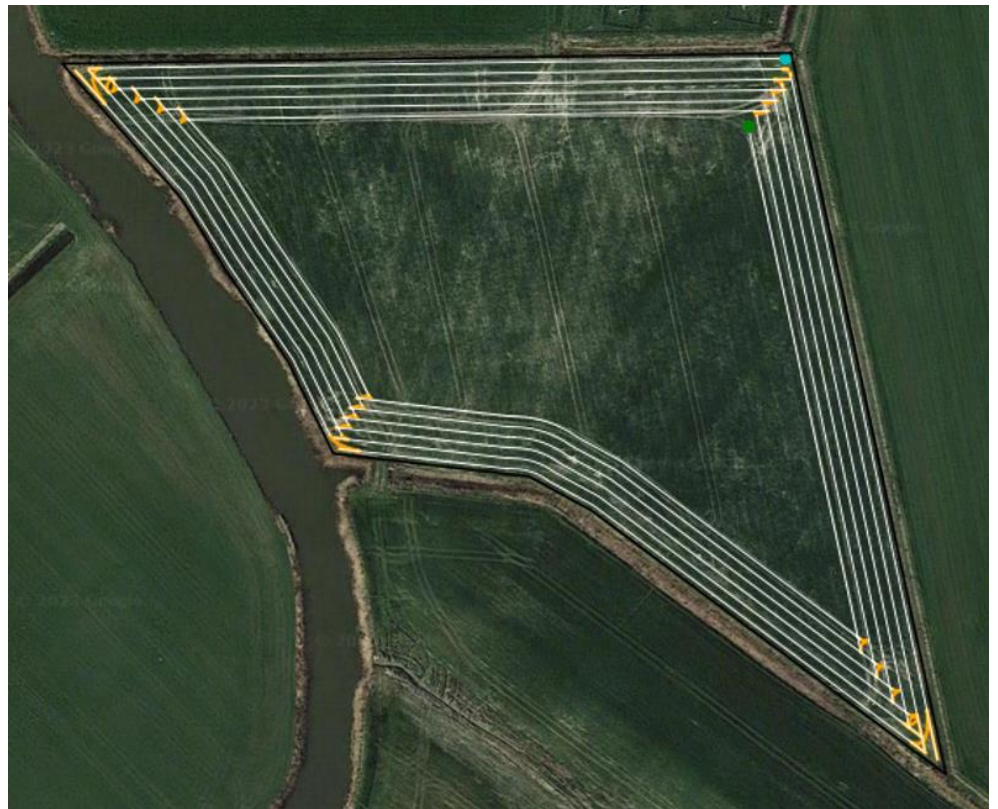
Geo-information Science and Remote Sensing

Thesis Report GIRS-2023-09

Coverage Path Planning on Headlands for Autonomous Field Operations

Rick Fennema

16 March 2023



WAGENINGEN
UNIVERSITY & RESEARCH



Coverage Path Planning on Headlands for Autonomous Field Operations

Rick Fennema

Registration number:

1012138

Supervisors:

Dr.ir. S. (Sytze) de Bruin
Gonzalo Mier Muñoz

A thesis submitted in partial fulfilment of the degree of Master of Science
at Wageningen University and Research,
The Netherlands.

16 March 2023

Wageningen, The Netherlands

Thesis code number: GRS-80436

Thesis Report: GIRS-2023-09

Wageningen University & Research

Laboratory of Geo-Information Science and Remote Sensing

Abstract

Justification: In agriculture, labour shortage is becoming more and more of a problem. Furthermore, the increasing weight of the machinery is also increasing soil compaction, which can lead to lower yields. A possible solution to overcome these problems is to use light-weight robots.

Aims: These robots require Coverage Path Planning (CPP) for covering agricultural fields. Much research has already been done on CPP. However, a CPP on headlands is understudied. Therefore, this study aimed to find important design criteria for creating a headland CPP, concerning the width of the headland and required turning manoeuvres, which also deals with the dimensions of the robot-implement combination. Moreover, a headland CPP is proposed in this study.

Methods: The headland CPP in this study is based on a robot with a rear-mounted implement, where the field operation is a seeding or tillage-like operation. Furthermore, the basis of the headland CPP uses a fishtail pattern.

Results and Discussion: The headland CPP is focused on the field corners, which requires a Corner Planning Approach (CPA) for covering the corner area. In this study, two different CPAs are created, which are focused on either a higher coverage or a smaller travelled distance for the corner. For each field corner, the optimal CPA is selected based on the non-covered area and the travelled distance. However, under certain circumstances, the CPAs create infeasible turning manoeuvres.

Conclusions: The most important design criterium for creating a headland CPP is to avoid crossing the field border. Therefore, the physical dimensions of the robot-implement combination are required when designing a turning manoeuvre and determining the headland width. Furthermore, a two-dimensional working area is required to allow proper coverage of the headland by the implement. Moreover, the headland width should be determined using all robot-implement combinations needed for a growing season to ensure feasible turning manoeuvres for all robot-implement combinations.

Synthesis: When creating a (headland) CPP, it is important to take the dimensions of the robot-implement combination into account, because of the swinging behaviour of the implement. Furthermore, for the start and end locations of the paths of a field operation, it is important to take into consideration that the implement is normally not in the same position as the center of rotation, for which the path is defined. This is important to maximize the field coverage.

Preface

For the Master Biosystems Engineering, I had to write a thesis, which I conducted at the laboratory of Geo-information and Remote Sensing from the 5th of September 2022 until the 17th of March 2023.

During the process of writing the thesis, I had a lot of help and guidance from my supervisors. Therefore, I would like to thank Sytze de Bruin and Gonzalo Mier Muñoz for their supervision. Furthermore, I would also like to thank Chris Bulthuis for the many conversations we had about the thesis. Lastly, I want to thank Jack de Winter, Jeroen Fennema, Geert van Maldegem, and several other people for their talks and advice regarding my thesis.

Rick Fennema

Source from the background of the figure on the cover page: Google Maps (2023)

Table of Contents

- 1 Introduction ----- 1
 - 1.1 Soil compaction and shortage of labour ----- 1
 - 1.2 Possible solution ----- 1
 - 1.3 Development of route planning systems ----- 1
 - 1.4 Problem definition ----- 3
 - 1.5 Research questions ----- 3
- 2 Materials and Methods ----- 4
 - 2.1 Agricultural background and used concepts ----- 4
 - 2.2 Schematic overview for headland coverage path planning ----- 5
 - 2.2.1 Determine headland width ----- 5
 - 2.2.2 Corner Planning Approach ----- 5
 - 2.2.3 Headland Coverage Path Planning ----- 6
 - 2.3 Determining headland width ----- 8
 - 2.3.1 Required dimensions ----- 8
 - 2.3.2 Minimum width required for turning manoeuvres ----- 9
 - 2.3.3 Required headland width ----- 14
 - 2.4 Headland Corner Planning Approaches ----- 15
 - 2.4.1 FishTail Corner Planning Approach ----- 15
 - 2.4.2 Continuous Corner Planning Approach ----- 27
 - 2.4.3 Calculate the non-covered area of a turning manoeuvre ----- 29
 - 2.4.4 Choose the optimal Corner Planning Approach ----- 30
 - 2.4.5 Reprojection of the Corner Planning Approach ----- 31
 - 2.5 Headland Coverage Path Planning ----- 32
 - 2.5.1 Start and finish location at the start corner ----- 32
 - 2.5.2 Route generator ----- 33
- 3 Application of the methodology to a variety of dimensions and settings ----- 34
 - 3.1 Assessment of individual turning manoeuvres for a Corner Planning Approach ----- 34
 - 3.1.1 Assessment of free space FishTail Corner Planning Approach ----- 35
 - 3.1.2 Assessment of limited space FishTail Corner Planning Approach for convex corners - 36
 - 3.1.3 Assessment of limited space FishTail Corner Planning Approach for concave corners 37
 - 3.1.4 Assessment of Continuous Corner Planning Approach ----- 38
 - 3.1.5 Assessment of the objective function ----- 40
 - 3.2 Assessment of the route generator for headland Coverage Path Planning ----- 40
 - 3.2.1 Settings for the headland Coverage Path Planning ----- 40

3.2.2	The functionality of the route generator for headland Coverage Path Planning-----	42
4	Discussion-----	43
4.1	Important dimensions of a RIC for headland Coverage Path Planning-----	43
4.2	Design criteria for headland width-----	43
4.3	Design criteria for headland Coverage Path Planning turning algorithms-----	44
Proposed solutions	-----	44
Implications	-----	44
4.4	Application of objective function and headland Coverage Path Planning-----	45
5	Conclusion and recommendations-----	46
References	-----	47
Appendix Algorithms	-----	50
Appendix A	-----	55

List of abbreviations and commonly used terms

Name	Description	First section used
Field border	The border of the whole field	1.3
Headland	Area mainly used for turning manoeuvres at the field border (Figure 2)	1.3
Inner field	= Field border – Headland area. Main part of the field normally consisting out of a straight driving direction (Figure 2)	2.1
Path	The trajectory or route of the center of rotation from the RIC	2.1
Swath	The area the RIC covers with the implement when driving over the path	2.1
RIC	Robot-implement combination	2.2.1
Current swath number	The headland consists of an integer number of swaths. The current swath number tells at which swath the focus is at that step.	2.2.2
Field corner	A corner of the field border	2.2.2
Operation direction	Clockwise or counter-clockwise direction of the field operation	2.2.3
w_{robot}	Width of the robot	2.3.1
d_{crf}	Distance between the center of rotation and the front side of the robot	2.3.1
d_{crr}	Distance between the center of rotation and the rear side of the robot	2.3.1
d_{cri}	Distance between the center of rotation and the front side of the implement	2.3.1
d_{wa}	Distance from the front side of the implement to the front side of the working area	2.3.1
l_{im}	Length of the implement	2.3.1
l_{work}	Length of the working area	2.3.1
w_{im}	Width of the implement	2.3.1
w_{work}	Width of the working area	2.3.1
off_{im}	Offset of the implement orthogonal to the driving direction	2.3.1
off_{work}	Offset of the working area orthogonal to the driving direction	2.3.1
Working area	The area the implement needs to perform its operation. Defined by w_{work} and l_{work} .	2.3.1
Center of rotation	Represents the path of the RIC. More information is in section 2.3.1.	2.3.1
Corner points (of the RIC)	These points describe the dimensions of the RIC. They describe the robot, the implement, and the working area. They are found in Table 1.	2.3.1
Arriving pass	A line parallel to the part of the field border where the RIC drives over when arriving at the field corner.	2.3.2
Center of the curve	The location around which the RIC rotates	2.3.2
IpA	Limiting corner point on the RIC that determines Point A	2.3.2
IpB	Limiting corner point on the RIC that determines Point B	2.3.2
Limiting point	A corner point that limits the specific type of operation and therefore determines that part of the operation.	2.3.2
Point A	The start location of a turning manoeuvre. At this location, the implement stops doing its work.	2.3.2
Point B	The end location of a turning manoeuvre. At this location, the implement starts doing its work.	2.3.2

R	The minimum turning radius of a RIC.	2.3.2
CPA	Corner planning approach	2.4
α_{int}	The angle between the intersection of the arriving and leaving pass.	2.4.1.2
$F_i, i = 1, 2, \text{ or } 3$	Correction factors that depend on the value of α_{int}	2.4.1.2
Leaving pass	A line parallel to the part of the field border where the RIC drives over when leaving the field corner.	2.4.1.2
w_{LA}	Limiting width that influences Point A. This distance is calculated out of the leaving pass.	2.4.1.2
w_{LB}	Limiting width that influences Point B. This distance is calculated out of the arriving pass.	2.4.1.2
Free space FT-CPA	Free space fishtail corner planning approach. Aim: always full coverage of the swath.	2.4.1.3
Field limit	The RIC might cross the field border until the field limit.	2.4.1.4
Limited space FT-CPA_{cv}	Limited space fishtail corner planning approach at convex corners. Aim: never crossing the field border.	2.4.1.4
limited space FT-CPA_{cc}	Limited space fishtail corner planning approach at concave corners. Aim: never crossing the field border.	2.4.1.5
α_c	The angle of the field corner. (convex when $\alpha_c < \pi$, concave when $\alpha_c > \pi$)	2.4.2
C-CPA	Continuous corner planning approach. Aim: continuing the working operation without lifting the implement.	2.4.2
Minimum effective working width	When using the C-CPA, the working width decreases and is depending on the turning radius. With minimum effective working width, the minimum turning radius is determined (section 2.4.2).	2.4.2
Work radius	The radius required for the C-CPA, which can be determined using the minimum effective working width	2.4.2
Corner angle	Angle of a field corner	3.1.1

1 Introduction

1.1 Soil compaction and shortage of labour

Agriculture in developed countries is facing multiple problems at the same time, for example, a shortage of skilled labour and soil compaction (Christiaensen et al., 2020; Nawaz et al., 2013). The soil compaction is mainly caused by the increasing size of agricultural machinery (McPhee et al., 2015). Due to soil compaction, crop yields are prone to decreases of 10% to 15% (Godwin et al., 2019). Furthermore, soil compaction increases the needed energy for tillage operations by 200% to 300%, which leads to greater fuel consumption and hence increased costs (Diserens et al., 2014; Godwin et al., 2019). Moreover, soil compaction decreases the infiltration rates significantly, leading to a slower uptake of water (Godwin et al., 2019). This can lead to flooded areas, which can harm crop yields (Scott et al., 1989).

The increasing size of agricultural machinery is a result of mechanization in agriculture (Parvin et al., 2022). The main benefit of the technical revolution is the substantial improvement of efficiency in agriculture (Parvin et al., 2022). However, Christiaensen et al. (2020) state that developed countries evolved from having enough skilled labour to a shortage of skilled labour during the mechanization of agriculture. Therefore, the positive effect of mechanization in agriculture also has some downsides related to skilled labour needs. Nowadays, the European Union still has a shortage of especially seasonal agricultural workers (Augère-Granier, 2021).

1.2 Possible solution

A possible solution to overcome the problems of soil compaction and a shortage of skilled labour is to use a relatively light-weighted robot, which can drive a pre-defined route (de Bruin, 2022). With the use of a robot, field operations require less time of the farmer, because the robot can work autonomously in the field once it is properly installed. Furthermore, a light weighted robot will cause less soil compaction. By optimising the route of the robot, the soil contact as a result of the driven path is minimized, which will also lead to lower soil compaction of the whole field (Zhai et al., 2020). By using an autonomous robot, the two problems can be dealt with at the same time.

1.3 Development of route planning systems

For a robot to autonomously operate in a field, a guidance system is needed. A widely used guidance system in agriculture is a GPS guidance system. The earliest form of GPS systems only indicate the offset from a given line using a lightbar and the operator of the tractor had to manually steer to follow the set path (Heraud & Lange, 2009). These earliest GPS guidance systems were not able to autonomously turn on the headland and avoid obstacles. Headlands are the parts of the field that are used for turning. Nowadays automated headland turns and obstacle avoidance are also available, which makes it suitable to create an autonomous route (Heraud & Lange, 2009). These options can avoid unnecessary driving over the field, which results in lower soil compaction. Furthermore, the driver can focus more on the actual work; the functioning of the implement (Fendt, 2022).

More and more options became available to drive the desired route in different ways, see Figure 1. Nowadays it is also possible to store very complex paths to be used for the next operation (Fendt, 2022). However, a disadvantage is that all these options require time to set up and need to be manually created by physically driving along the border of a field or driving across the field to create the guidance paths. Each type of pattern needs to be manually selected and the number of headland passes also needs to be indicated. Furthermore, most of these options require additional payment to unlock them (AGGPS, 2022; Sloans, 2018).

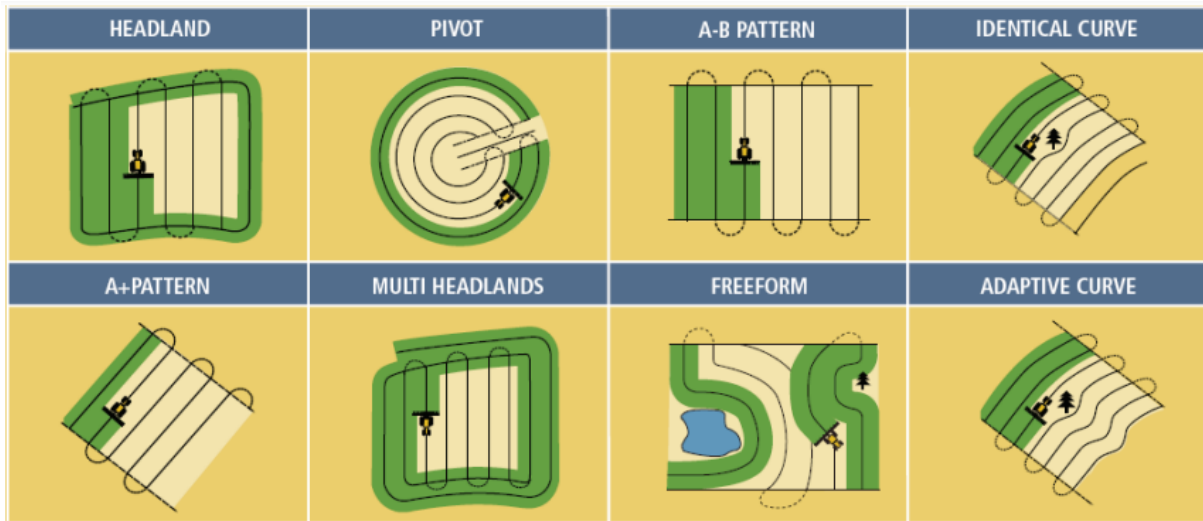


Figure 1: Different guidance paths which are currently available. This figure shows that it is possible to create paths with very complex shapes (Heraud & Lange, 2009).

Nowadays companies are producing autonomous tractors which can fully cover the field, like AgXeed, John Deere, and Case IH (AgXeed, 2022a; Case IH, 2022; John Deere, 2022). These companies claim they are at the start of mass production. Their autonomous tractors underwent substantial testing to ensure they fulfil the safety requirements. To reach the safety requirements, these autonomous tractors are equipped with many sensors to ensure unwanted collisions in the field. However, the route optimisation software created by these companies is not publicly available. Therefore, this software cannot be used by other people to create a coverage path planning (CPP). A CPP creates a route for a vehicle that can fully cover a field and avoid obstacles (Galceran & Carreras, 2013).

Much research has been done on CPP. Chakraborty et al. (2022) report several studies allowing the creation of a CPP for complex and irregularly shaped fields. These studies used different objective functions for optimising the CPP, for example, fuel consumption, overlap and skipped field parts, and travelled distance. Furthermore, Chakraborty et al. (2022) state that the best CPP approach depends on the type of operation on the field (e.g. sowing, harvesting). Unfortunately, the CPP approaches found only describe the largest part of the algorithm and are therefore missing important details. Therefore, it is hard to implement these CPP approaches in a new robot.

However, a new project is initiated for creating and optimising a CPP, which is called the Fields2Cover project (de Bruin, 2022; Mier, 2022; Mier et al., 2023). This project aims to (1) integrate already existing knowledge for route planning optimisation; (2) accomplish new developments, and (3) create and publish it as an open-source software library, to make it easier for other developers to work on CPP. This software library can deal with complex field shapes and is still under construction for more options, e.g. planning routes for multiple robots working simultaneously. At the moment of writing, the Fields2Cover project is able to create a CPP for the field, except for the headland. The headland is only used for turning manoeuvres and is therefore not covered by the CPP.

For creating the CPP from the Fields2Cover project, a headland width is needed as input. Jin and Tang (2010) developed a method to determine the minimum required headland width. However, this method is only based on the width of the implement and does not take the dimensions of the implement and tractor into account. The out-swinging behaviour of an implement attached to a tractor at some distance from the point of rotation was not taken into account. To determine a more realistic minimum required headland width, the representation of the implement and robot has to be further elaborated.

Nilsson and Zhou (2020) also defined a simple approach to determine the headland width. Their headland width is based on the authors' experience, and they state that it can be used for most fields. This indicates that their approach does not always create a feasible headland width. Nilsson and Zhou (2020) also created an algorithm for covering the headland area. Unfortunately, they also do not take the dimensions of the implement and tractor into account. Therefore, the field border is crossed in reality when using this algorithm. Furthermore, their paths on the headland are smoothed in the corners, resulting in non-covered areas. Therefore, Nilsson and Zhou (2020) say a full coverage of the headland requires more advanced turning algorithms, which include reverse driving.

1.4 Problem definition

The creation of CPPs has been extensively studied. However, computer code for creating these CPPs is not publicly available or needs to be created from other studies. Furthermore, many studies only focus on a small part of the optimisation problem for a CPP, hindering comprehensive and wide applicability. Fortunately, the Fields2Cover project is starting to integrate already existing knowledge into an open-source library. This library is always under construction, which gives room for adding new functionalities.

The CPP algorithms found by Chakraborty et al. (2022) focus on optimising a field where the headlands were only used for turning. The creation of the headland CPP is understudied; no study was found on feasible optimising algorithms that can autonomously determine the width and path planning of the headland. Currently, creating a CPP for each field operation involves manual work to create the width and path planning of the headlands. This is inconvenient when aiming for automated solutions.

Furthermore, no study was found that took the dimensions of the implement and robot into account when creating a CPP. The studies found only focused on the working area from the implement. Therefore, unwanted collisions and crossing of the field border can occur. Moreover, there is a lack of turning algorithms enabling reverse driving in headland corners, which also concerns the limitations of the headland corner. Therefore, the optimisation of headland corners disregards important options.

1.5 Research questions

The objective of this study is to find an optimised solution for determining the width and the path planning of the headlands autonomously when also considering the dimensions of the robot and implement. These solutions are aimed to be integrated into the Fields2Cover library. This results in the following research questions:

1. What are the important dimensions of a robot and implement for creating a CPP on headlands?
2. What are the design criteria for determining the headland width?
3. What are the design criteria for turning algorithms in headland corners that include reverse driving?
4. What is the outcome of the objective function implementing (1-3) with different settings and dimensions?

2 Materials and Methods

In this section, the methodology to get answers to the research questions in section 1.5 is explained. Section 2.1 is about the agricultural background and used concepts to understand the design criteria for headland planning. Section 2.2 shows a schematic overview of how the headland CPP is created in this study, together with a brief description of the schematic overview. Section 2.3 is about determining the headland width based on its design criteria. Section 2.4 describes two different headland corner planning approaches, which are used in this study for path planning on the headland. Finally, section 2.5 describes how the headland CPP is generated and put together.

2.1 Agricultural background and used concepts

To create design criteria for headland planning, it is important to understand the reasonings of the farmers and how agricultural machinery works. Furthermore, every agricultural field is unique. Most fields have their own shapes and different field entry locations. Moreover, fields can be surrounded by many obstacles like trees and ditches. Even inside fields, there can be obstacles. Therefore, the characteristics of the CPP need to be determined for every single field.

Before a crop is seeded, the seedbed needs to be prepared, to create good conditions for the seeds to grow. The seedbed preparation in the Netherlands usually involves tillage operations like cultivating or ploughing. When the seedbed is prepared, farmers try to avoid driving over the prepared seedbed before the crop is seeded. Therefore, seeding operations usually start with seeding the inner part of the field and using the headland for turning (Figure 2). Hence, the inner field needs to be prepared and seeded before the seedbed is prepared on the headland (G. van Maldegem, Personal Communications). A different way of seeding the whole field is to prepare the seedbed for the whole field and start seeding with the headland before seeding the inner field (J. Fennema, Personal Communications). Therefore, because the crop is already seeded on the headland, the seedbed on the headland is not damaged. This is only possible when the growing environment of the crop is not damaged when the tractor/robot is turning on the headland for seeding the inner field. Therefore, the seeding operation depends on the crop type.

The seeding pattern normally depends on the sprayer and the harvester, especially for row crops like potatoes. For a sprayer, it is important to not cross the field border with the spray boom, because this can cause unwanted collisions. Furthermore, in the Netherlands, there are regulations about crop-free zones next to ditches which depend on the type of sprayer (Agrotheek, 2023). A sprayer must not operate within this crop-free zone. Moreover, a sprayer needs a path without many bumps to ensure good spraying quality (J. Fennema). Therefore, farmers usually use parts of the path from the seeder for the sprayer to avoid bumps from for example potato ridges. The seeding pattern must also make it possible to be able to harvest as much as possible, and limit the driving over unharvested crops, to ensure the highest profit possible.

The width of agricultural machinery is dependent on the type of farm and the type of operation. A sprayer usually has a different width than a seeder or a plow. For reasons of compatibility, machine widths are normalized, to make sure a sprayer can drive through the crops without damaging them (van Velde, 1998). However, the normalized widths can cause for particular crops the machinery to be asymmetrically attached to the tractor/robot and therefore located a bit more to the left or right (van Velde, 1998).

In this study, some concepts are regularly used, which are shown in Figure 2. The field consists of two different areas; the headland and the inner field. The headland is used for turning manoeuvres to go from one swath of the inner field to another. A swath is the area covered by the implement while the

robot is driving over the path. The direction the front side of the robot is facing is called the heading direction. The swaths on the inner field normally consist of straight lines next to each other. The swaths on the headland follow the field border. If the field border has a curved section, then the swaths on the headland follow this curved section. The field border is described by vertex points. A curved section of the field border thus is not a continuous curve but is discretized; the field geometry is determined by vertex points describing the field border. For each vertex point describing the field border, the direction of the swath on the headland changes. Therefore, a turning manoeuvre is required. The vertex points of a curved section also require turning manoeuvres to allow for a change in heading direction. In this study, the headland CPP focuses on the turning manoeuvres at the vertex points of the field border.

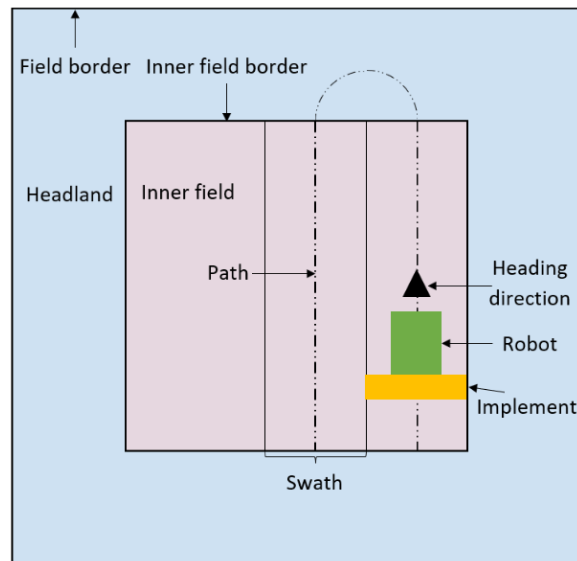


Figure 2: Commonly used concepts in this study.

2.2 Schematic overview for headland coverage path planning

In this section, a schematic overview of the headland CPP is given (see Figure 3). This schematic overview shows the main structure of how the headland CPP is determined in this study. The detailed descriptions of the functions used are found in further sections in chapter 2 Materials and methods. Below, a small description is given about the schematic overview.

2.2.1 Determine headland width

It is important to know the width of the headland because every Robot-Implement Combination (RIC) should be able to operate on the field. Therefore, the headland width needs to be determined first. The headland width is calculated for all the RICs used over a full growing season, and then the maximum needed headland width is selected (section 2.3). Based on the headland width, the number of swaths on the headland is determined.

2.2.2 Corner Planning Approach

The headland CPP requires the coordinates of the field boundary and the start corner at the field boundary. The start corner is the field corner which is closest to the field entry location, and is the start and end location of the headland CPP. The headland CPP starts either at the inner field border or the field border, depending on the type of operation (section 2.5). In this study, the headland CPP uses a spiral pattern, where the pattern moves either further inwards or outwards the field, from one swath number of the headland to the next (section 2.5). This inward or outward movement of the headland

CPP occurs at the start corner. Each field corner requires a Corner Planning Approach (CPA) that connects the swaths of the headland in each corner with a specific turning manoeuvre.

In this study, two generic turning options for the CPA are considered. These are the FishTail CPA (FT-CPA) and the Continuous CPA (C-CPA). A detailed description of the FT-CPA is found in section 2.4.1, and a detailed description of the C-CPA is found in section 2.4.2. The main difference between the two is that the FT-CPA uses a back-and-forth turning manoeuvre with a lifted implement, whereas the C-CPA continues a forward-driving motion and maintains a lowered implement. The optimal CPA is selected for each field corner based on the non-covered area and the travelled distance (section 2.4.4). The start corner always uses an FT-CPA, because of the changing swath number (section 2.5). Each field corner has the same amount of turning manoeuvres as there are swaths on the headland.

The calculation for the FT-CPA and the C-CPA uses a locally oriented, relative coordinate system (sections 2.4.1.7 and 2.4.2). Therefore, the CPA is reprojected to place the CPA into the field at the correct place (section 2.4.5).

2.2.3 Headland Coverage Path Planning

Once the optimal CPAs for all corners are known, a route is generated. The route depends on the start border and the operation direction (clockwise or counter-clockwise). The route starts at either the inner field border or the field border. The route is determined by logically ordering the part of the CPAs, which also concerns the operation direction.

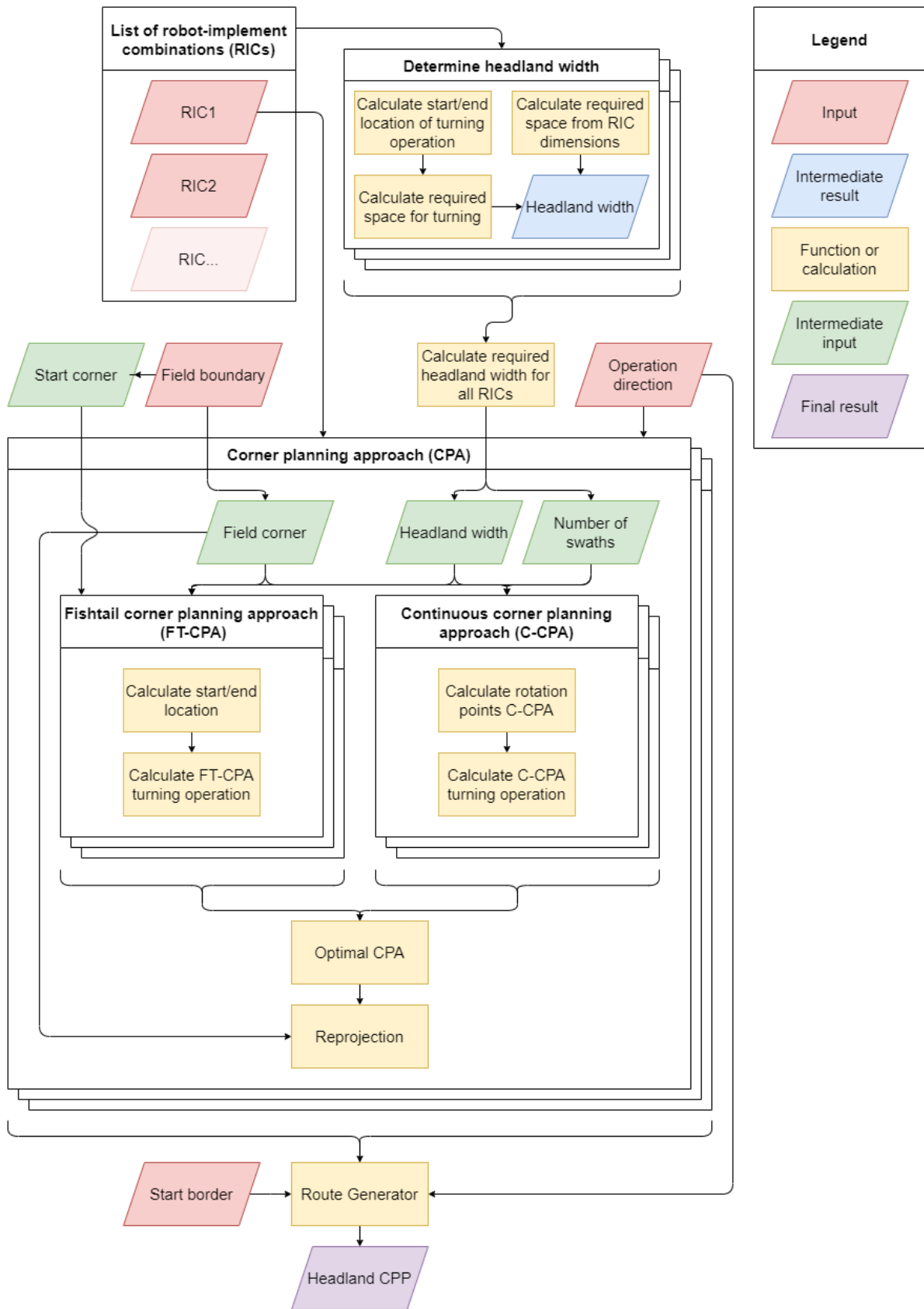


Figure 3: Schematic overview for headland path planning using the FishTail and Continuous Corner Planning Approach. Created with DrawIO (2023).

2.3 Determining headland width

The headland width must have a minimum width to allow turning manoeuvres of the inner field for every RIC used over a growing season. This section explains how the headland width is determined based on multiple RICs.

2.3.1 Required dimensions

The minimum headland width is either determined by half the width of the implement (e.g., a spray boom) or by the minimum width required for turning manoeuvres. To determine the latter, it is important to know the dimensions of the RIC, which are shown in Figure 4. The shown dimensions also play a role in the corner planning, which is described in section 2.4. All the paths planned in this study refer to the location of the center of rotation from the RIC. The center of rotation is the location on the center line of the RIC (Figure 4) that has a perpendicular angle between the driving direction and the turning radius of the RIC (Scheuer & Fraichard, 1997). In this study, the center of rotation always refers to the center of rotation of the RIC.

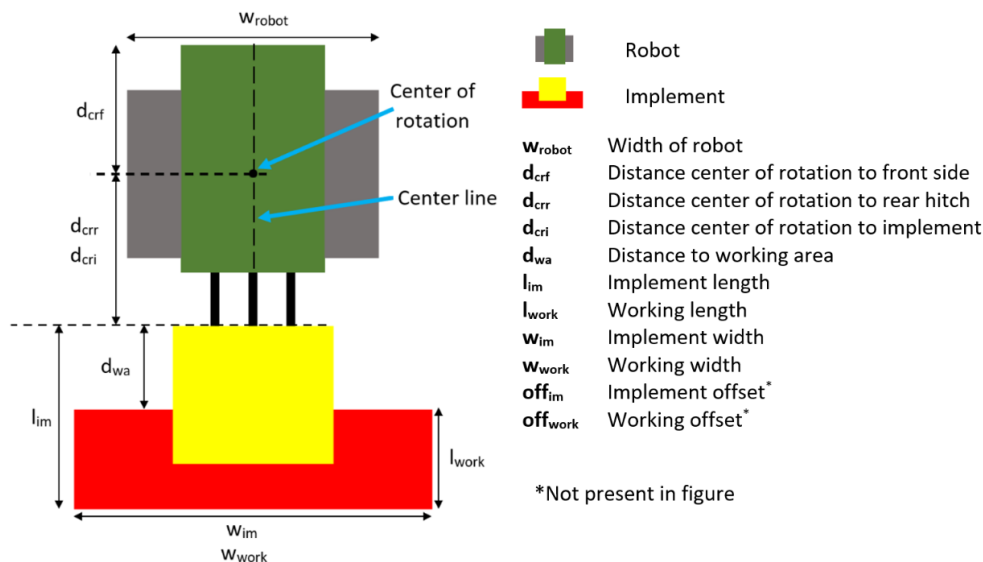


Figure 4: Dimensions needed from a RIC to determine the minimum width required for turning manoeuvres on the headland. The offsets have a positive value when they are to the left of the center of rotation. The offset shifts the implement width or working width to the left or right.

Often, the working width of the implement is equal to the implement width. However, this is not always the case. For example, a two-row potato harvester from GRIMME has a smaller working width (1.5 m) than the implement width (3.3 m) (GRIMME, 2022; Horsmans, 2023). Furthermore, this potato harvester is not centred on the rear of the tractor but it has an offset. This offset was also considered in the current study (off_{im} and off_{work} , see Figure 4). Combining the working width with the working length results in the working area. This area is needed for the implement to apply its operation. The working width can also be wider than the implement width. For example, the fertilizer spreader Accura 1600 from KUHN has an implement width of 2.37 m and a working width varying between 12 to 36 m (KUHN, 2023).

In this study, the furthest corner points of the RIC are important, because they influence the paths on the headland. These corner points constrain the headland planning. Table 1 lists the corner points and their coordinates in the local coordinate system. Note that the distance d_{cri} is signed, depending on the location of the implement relative to the robot. When the implement is behind the robot, the distance d_{cri} is positive, but it is negative when the implement is in front of the robot.

Table 1: Corner position of every corner from a RIC, where the origin is the center of rotation, the x-axis is the heading direction of the RIC, and the y-axis is orthogonal to the x-axis. The left side of the RIC is the positive y-axis.

Corner position	Abbreviation	x	y
Front right robot	FRR	d_{crf}	$-0.5 * w_{robot}$
Front left robot	FLR	d_{crf}	$0.5 * w_{robot}$
Rear right robot	RRR	$-d_{crr}$	$-0.5 * w_{robot}$
Rear left robot	RLR	$-d_{crr}$	$0.5 * w_{robot}$
Front right implement	FRI	$-d_{cri}$	$-0.5 * w_{im} + off_{im}$
Front left implement	FLI	$-d_{cri}$	$0.5 * w_{im} + off_{im}$
Rear right implement	RRI	$-d_{cri} - l_{im}$	$-0.5 * w_{im} + off_{im}$
Rear left implement	RLI	$-d_{cri} - l_{im}$	$0.5 * w_{im} + off_{im}$
Front right working area	FRW	$-d_{cri} - d_{wa}$	$-0.5 * w_{work} + off_{work}$
Front left working area	FLW	$-d_{cri} - d_{wa}$	$0.5 * w_{work} + off_{work}$
Rear right working area	RRW	$-d_{cri} - d_{wa} - l_{work}$	$-0.5 * w_{work} + off_{work}$
Rear left working area	RLW	$-d_{cri} - d_{wa} - l_{work}$	$0.5 * w_{work} + off_{work}$

2.3.2 Minimum width required for turning manoeuvres

To go from one swath of the inner field to another, a turning manoeuvre is required on the headland. In this study, the turning type Dubins curve is used to determine the minimum width required for turning manoeuvres (Dubins, 1957). Dubins curves employ a given turning radius and use a forward motion only. A Dubins curve connects two points with each a certain heading direction, and a given turning radius by the shortest driving distance possible for a forward driving direction (Dubins, 1957). This is done by combining different combinations of a left turn L, a right turn R, and a straight part S. E.g., an RSL is a right turn, straight part, and left turn. Examples of these combinations are shown in Figure 5. However, not all the different manoeuvres shown in Figure 5 have to be used for determining the headland width, because it contains both a left and a right turn, which are mirrored versions of each other and will therefore end up with an equal minimum required headland width. In this study, only the right turn Dubins curve configurations RSR, LRL, and RSL are used for determining the minimum width required for headland turning (see Figure 6). The Dubins curve configuration used depends on the dimensions and minimum turning radius (R) of the RIC.

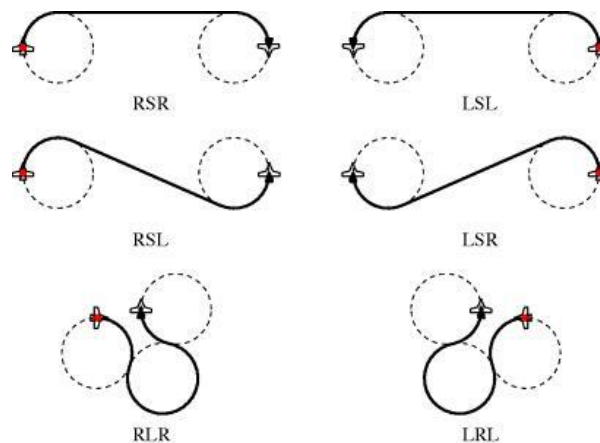


Figure 5: Different configurations for the Dubins curve. The red plane is the starting point (Schouten, 2022).

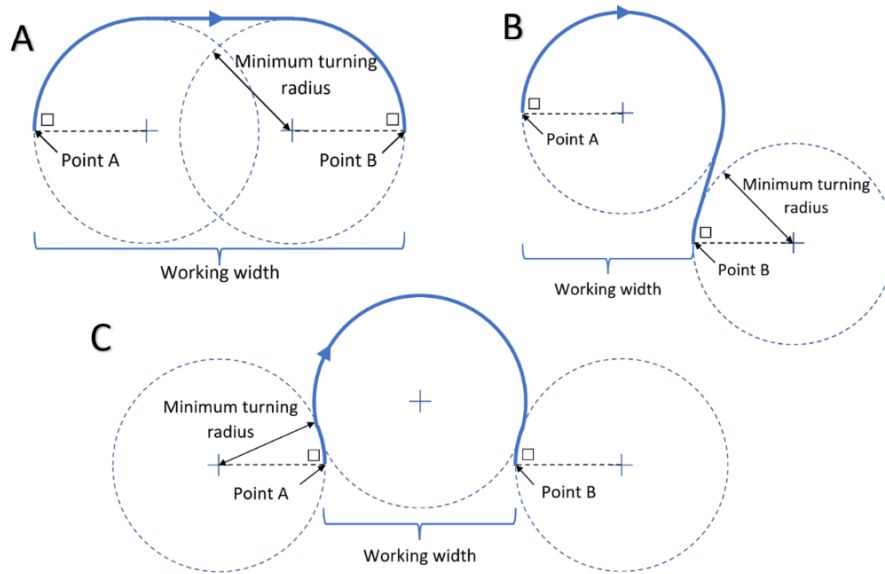


Figure 6: Feasible Dubins curve configurations for turning to a right-sided adjacent pass. (A) is an RSR configuration, (B) is an RSL configuration, and (C) is an LRL configuration.

To determine the minimum headland width required, the Dubins curve is planned for two adjacent passes, where the RIC goes from Point A to Point B, with Point B on the right side of Point A (Figure 6). The minimum headland width consists of two parts: (1) the distance from the inner field border to the center of the curve, and (2) the distance from the center of the curve to the outer corner point of the RIC.

The angle between the heading direction and the inner field border is not always orthogonal. Furthermore, this angle influences the required headland width. To make sure that the CPP of the inner field is always feasible, a range from 0 to π rad (0-180°) was used for the angle between the heading direction and the inner field border to determine the minimum headland width. This varying angle also influences the needed Dubins curve configuration. Below, the right Dubins curve configuration and the calculations for the three different distances for the minimum headland width are explained in more detail.

2.3.2.1 Determining the right Dubins curve configuration

For determining the right Dubins curve configuration, the working width, the working offset, the R , and the distance between points A and B are required. The criteria for the right Dubins curve configuration are shown in Algorithm 1:

Algorithm 1: Select the right Dubins curve configuration

- IF $w_{work} - 2 * |off_{work}| \geq 2 * R$ THEN:
 - o RSR configuration
 - ELSEIF $d_{AB} \geq 2 * R$ THEN:
 - o RSL configuration
 - ELSE:
 - o LRL configuration
-

2.3.2.2 Distance from the inner field border to Points A and B

To determine the distance from the inner field border to the center of the curve, the locations for Points A and B are required first. The location Point A for starting the turning manoeuvre is not located on the inner field border but is determined by the dimensions of the RIC and the angle α_{int} between

the heading direction of a pass and the inner field border. To avoid soil compaction, the turning manoeuvres are limited to the headland in this study. Therefore, the robot needs to be on the headland during the turning manoeuvre. Hence, Point A is determined by either the rear of the working area or the rear of the robot, depending on the location of the implement on the robot. The rear from both the working area and the robot must have fully crossed the inner field border. This is shown in Figure 7 (A). Point B is determined similarly compared to Point A, but is determined by either the front side of the robot or the front side of the working area. Neither of these front sides can cross the inner field border at Point B. This is shown in Figure 7 (B).

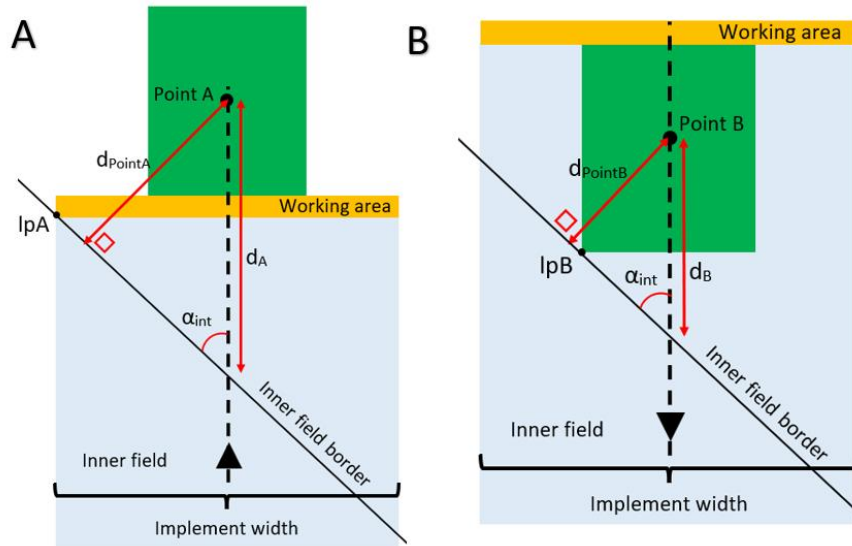


Figure 7: Dimensions used to calculate the distances d_{PointA} and d_{PointB} from the center of rotation to the inner field border for Points A and B. Points A and B are determined by the moment a point from the RIC is touching the inner field border when the RIC is on the pass. (A) shows how Point A is determined, (B) shows how Point B is determined.

To determine the distances d_{PointA} and d_{PointB} , the distances d_A and d_B need to be known. This is done using a part of Algorithm A-2 in the Appendix. A description of this algorithm is provided in section 2.3.1.1. Because the RIC at Point B is directed in the opposite direction compared to Point A, only the part for calculating Point A from Algorithm A-2 is used. This part also needs a value w_{LA} , which is used as an offset between the inner field border and the limiting point on the RIC touching the inner field border. This offset is not required for calculating the headland width and is therefore set to 0. Because Point B is directed in the opposite direction compared to Point A, all the coordinates from the limiting points on the RIC for Point B are multiplied by -1. In Table 2, the limiting points of the working area and the robot for Points A and B are found.

Table 2: Limiting points of the working area and the robot for calculating d_A and d_B . From each limiting point, the x-value is needed as input (x_{lpA}) and the y-value is needed as input (y_{lpA}). These limiting points are found in Table 1.

Angle α_{int}	Point A work	Point A robot	Point B work	Point B robot
0 to 0.5π	RLW	RLR	-FRW	-FRR
0.5π to π	RRW	RRR	-FLW	-FLR

For each Point A and B, either the working area or the robot is limiting. Based on the calculations using the values from Table 2, the distance of the limiting point is determined. This is done using the following procedure (Equations 1-2):

$$d_A = \max(d_{A-work}, d_{A-robot}) \quad [m] \quad (1)$$

$$d_B = \max(d_{B-work}, d_{B-robot}) \quad [m] \quad (2)$$

Using Equations 1-2, the distances d_{PointA} and d_{PointB} are calculated in Equations 3-4:

$$d_{PointA} = |d_A * \sin(\alpha_{int})| \quad [m] \quad (3)$$

$$d_{PointB} = |d_B * \sin(\alpha_{int})| \quad [m] \quad (4)$$

2.3.2.3 Offset from the furthest center of the curve to the inner field border

The next distance needed to determine the headland width is the distance between the center of the curve and the inner field border, which also includes the distance d_{PointA} or d_{PointB} . For the LRL, RSR, and RSL Dubins curve configurations the (first) R turn has the largest distance between the center of the curve and the inner field border. Because the RSR and RSL configurations both start with a right turn, they have the same procedure for calculating the distance. Therefore, they are named RS* in this study. For an RS* configuration, the offset for the center of the curve is calculated based on Point A or Point B. This offset for both Dubins curve configurations is calculated using Equation 5:

$$\begin{aligned} d_{offRS^*,A} &= \cos(\alpha_{int}) * R + d_{PointA} & [m] \\ d_{offRS^*,B} &= -\cos(\alpha_{int}) * R + d_{PointB} & [m] \\ d_{offRS^*} &= \max(d_{offRS^*,A}, d_{offRS^*,B}) & [m] \end{aligned} \quad (5)$$

where d_{offRS^*} is the offset from the center of the curve to the field border for an RS* configuration.

The offset for an LRL configuration cannot be calculated using Equation 5, because this configuration first starts with a left turn. In Figure 8, an LRL configuration is shown with its offset from the line parallel to the inner field border and going through Point A.

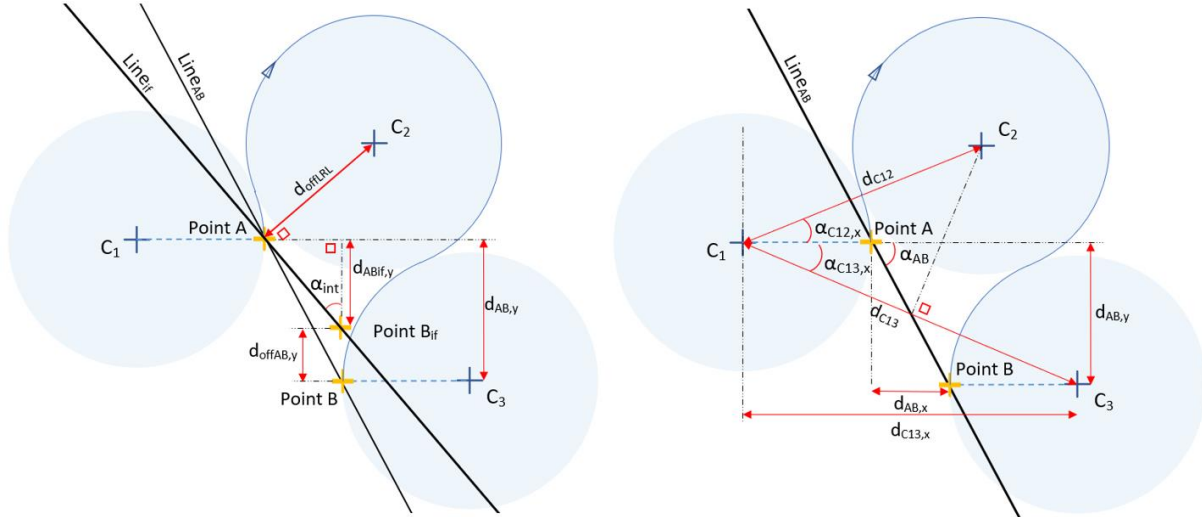


Figure 8: Dubins curve LRL configuration and the needed dimensions to determine the offset of the center from C_2 . This configuration starts at point A and ends at point B. $Line_{AB}$ is the line through Points A and B_{if} , and $Line_{if}$ is a line through Point A and parallel to the inner field border.

To calculate the distance d_{offLRL} in Figure 8, the equation for the distance between a point (C_2) and a line through two points (Points A and B_{if}) is used. Furthermore, the value d_{offLRL} is signed, because C_2 can also be on the other side of the line through Points A and B_{if} . Moreover, the distance d_{PointA} must also be added to obtain the distance between the inner field border and the center of the curve. Combining this information, the value for d_{offLRL} is calculated using Equation 6:

$$d_{offLRL} = \frac{(x_B - x_A)(y_C - y_A) - (y_B - y_A)(x_C - x_A)}{\sqrt{(x_B - x_A)^2 + (y_B - y_A)^2}} + d_{PointA} \quad [m] \quad (6)$$

where (x_A, y_A) = Point A, (x_B, y_B) = Point B_{if} , and (x_C, y_C) = Point C_2 .

Point B_{if} is different from Point B, because Point B_{if} is on the line through Point A and parallel to the inner field border. The calculations for Points A, B, B_{if} , and C_2 are found in Algorithm A-1 in the Appendix. For these calculations, the origin is Point C_1 , the y-axis is set to the direction of the arriving pass, and the x-axis is orthogonal to the y-axis.

2.3.2.4 Distance between the furthest corner of the RIC and the center of the turning curve

Now the distance between the inner field border and the furthest center of the curve is known, the distance between the center of the curve and the outermost point of the RIC during the Dubins curve turning manoeuvre is still to be determined. The two distances combined determine the minimum width required for the RIC. Four possible locations on the RIC can be the furthest point; these are listed in Table 3 and shown in Figure 9. The distances between the center of the curve and these locations are calculated using Equation 7, which uses the values from Table 3.

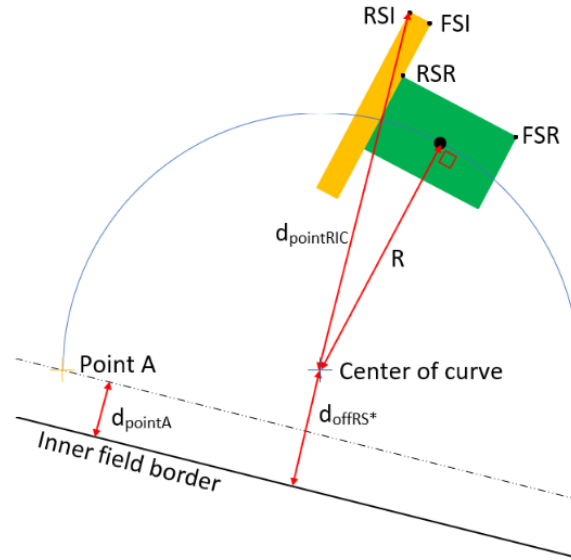


Figure 9: One out of the four points of the RIC in Table 3 has the furthest distance to the center of the curve. This figure also shows the distance d_{offRS^*} from the inner field border to the center of the curve for the RS^* configuration.

Table 3: Locations of the different possible furthest locations distanced from the center of the curve. The parameters are shown in Figure 4. The offset of the implement is set to an absolute value, because for either a left or a right turn the offset will be positive, and both turns should be feasible.

Location position	Abbreviation	x	y
Front side robot	FSR	d_{crf}	$R + 0.5 \cdot w_{robot}$
Rear side robot	RSR	d_{crr}	$R + 0.5 \cdot w_{robot}$
Front side implement	FSI	d_{cri}	$R + 0.5w_{im} + off_{im} $
Rear side implement	RSI	$d_{cri} + l_{im}$	$R + 0.5w_{im} + off_{im} $

$$d_{pointRIC} = \sqrt{x^2 + y^2} \quad [m] \quad (7)$$

where $d_{pointRIC}$ is the distance of a point (x, y) on the RIC to the center of the curve. The values for (x, y) are found in Table 3.

The largest distance of one of the four locations from Table 3 is set to the parameter $d_{pointRIC}$.

2.3.2.5 Minimum headland width for Dubins curve turning manoeuvre

Now the required distances are known, they are combined to find the minimum headland width. The combination depends on the angle α_{int} and the distance between Points A and B. The distance between Points A and B determines if an LRL or an RS* Dubins configuration is required (section 2.3.2.1). When the right Dubins configuration is selected, its corresponding distance between the center of the curve and the inner field border is calculated. Then, the distance $d_{pointRIC}$ is added, which together determines the minimum headland width for a specific angle α_{int} .

To know the minimum headland width for all different possible values of α_{int} , it is determined for 200 uniformly distributed angles for α_{int} , ranging from 0 to π rad. The greatest outcome for the minimum headland width for α_{int} gives the minimum required headland width for a Dubins curve turning manoeuvre for a specific RIC. An example where the angle α_{int} is varied for a specific RIC is shown in Figure 10.

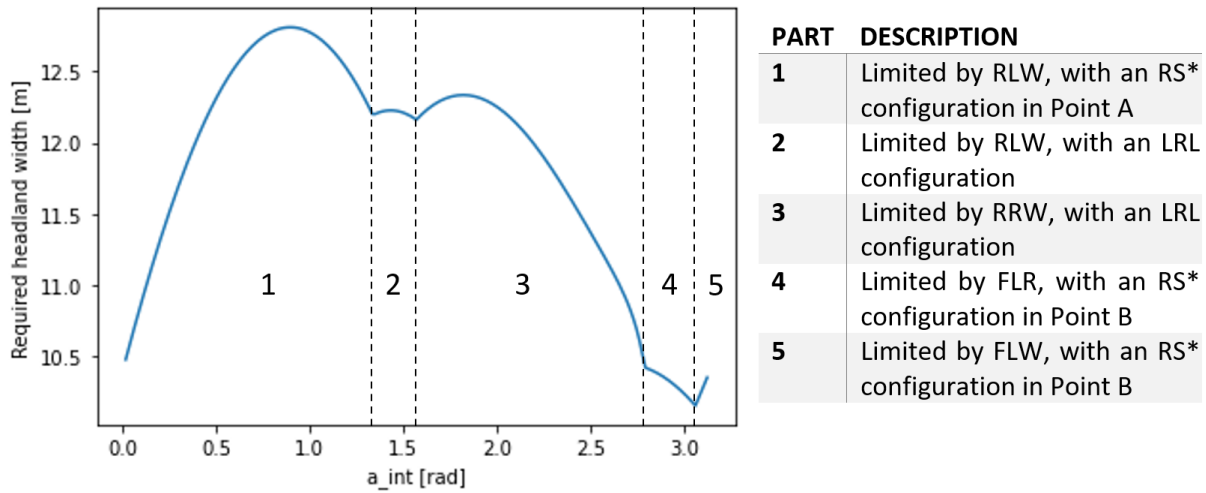


Figure 10: Example of the required headland width where the angle α_{int} is ranging between 0 and π . This figure is based on a RIC described in Table 11, section 3.

This minimum required headland width for a specific RIC needs to be determined for all the needed RICs during the growing season, except for a sprayer, because a sprayer uses a different turning principle. The minimum required headland width for a sprayer is determined in section 2.3.3. The greatest required headland width for all the RICs gives the final minimum required headland width for the turning manoeuvre.

2.3.3 Required headland width

The minimum required headland width is not only determined by the minimum width for turning manoeuvres but if used also by the width of the sprayer. Normally half the working width of the sprayer is used for covering the headlands while the other half is over the inner field. The spray boom is normally centred on the tractor. Therefore, half the width of the tractor/robot must also be considered to let the robot drive on the headland. This is required to avoid a bumpy path because otherwise one side of the robot would drive over the inner field. The minimum headland width for a sprayer is found using Equation 8:

$$d_{mhs} = \frac{1}{2} * (w_{work} + w_{robot}) + |off_{work}| \quad [m] \quad (8)$$

The highest value of either the minimum headland width for a sprayer or a turning manoeuvre determines the final minimum headland width (MHW).

2.3.3.1 Correction for working width(s)

Agricultural machines normally use standardized working widths, that match an integer number of times the minimum working width. Therefore, it is useful to have a headland width that is an integer multiplication of the working width to avoid large overlapping between the headland and the inner field. In this study, the working width of the seeder is used. This produces the final Equation 9 for determining the headland width:

$$w_{hl} = \left\lceil \frac{MHW}{w_{work}} \right\rceil * w_{work} \quad [m] \quad (9)$$

where w_{hl} is the headland width [m], and MHW is the minimum headland width [m].

2.4 Headland Corner Planning Approaches

For creating a headland CPP, the focus is on planning the field corners (see last paragraph Section 2.1). In this study, the headland CPP is based on a tillage or seeding operation, where the implement is attached to the rear of the robot. When making a CPA, the aim is to cover as much as possible with the implement, limit driving over already covered areas, and never cross the field border. Below, two different methods are described to cover a corner.

2.4.1 FishTail Corner Planning Approach

For some crops such as cereals, the seeding direction does not influence the harvesting direction. Therefore, the corner planning approach for seeding these crops is not directly dependent on the corner planning approach for harvesting. An example type for this corner planning approach is visible in Figure 11, which can be described as a FishTail Corner Planning Approach (FT-CPA). This FT-CPA has a circular pattern around the inner field border, where each round a new headland swath is covered. This approach allows a fast way to cover the headland with only a small distance required for turning in the corners.

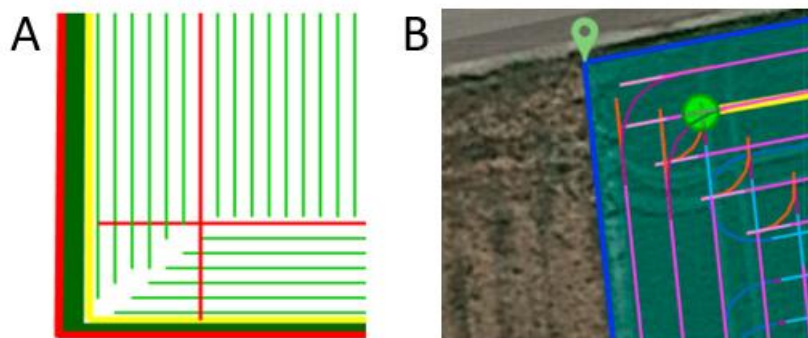


Figure 11: An FT-CPA based on literature (A) and an agricultural machinery manufacturer (B), which shows the same fishtail pattern for the corner planning approach (AgXeed, 2022b; de Bruin, 2011).

In Figure 11 (B), the connections between passes are different. This is because the RIC cannot pass the field border as it is constrained to remain within the field. This results in a different turn operation on the outer pass compared to the pass closest to the inner field. Therefore, the FT-CPA was divided into two subclasses; the free space FT-CPA and the limited space FT-CPA. In section 2.4.1.1 below, a schematic overview is shown that tells how the FT-CPA was determined. This section also refers to other sections about the detailed information of a function for creating an FT-CPA. Section 2.4.1.2 explains how a start and end location for an FT-CPA was determined.

2.4.1.1 Schematic overview of FishTail Corner Planning Approach

A schematic overview for calculating an FT-CPA is shown in Figure 12. The FT-CPA has three different approaches; the free space FT-CPA, the limited space FT-CPA_{cv}, and the limited space FT-CPA_{cc}. The free space FT-CPA is determined by the full coverage of the current swath (section 2.4.1.3). Therefore, this approach never has a non-covered area. However, when this approach is too close to the field border, it crosses the field border and therefore results in a non-feasible solution. Therefore, the required space is calculated, to find the minimum number of swaths needed for the turning manoeuvre without crossing the field border (section 2.4.1.6). To determine the required space, the operation direction of the field corner is needed. This tells if the field border is on the left or the right side of the RIC. When the free space FT-CPA requires more space than is available, a limited space FT-CPA_{cv} is used at a convex field corner, and a limited space FT-CPA_{cc} is used at a concave field corner.

When a field corner is convex and the free space FT-CPA does not fit, the limited space FT-CPA_{cv} is used. The main function of the limited space FT-CPA_{cv} is to never cross the field limit (section 2.4.1.4). The field limit is determined by the maximum distance the RIC might cross the field border, which is called d_{fl} (section 2.4.1.4). This crossing of the field border is required because an implement attached to the rear of a robot swings out during a turning manoeuvre. With the limited space FT-CPA_{cv}, the crossing of the field border is never larger than d_{fl} . Because the limited space FT-CPA_{cv} is limited by the field border, the current swath is not always fully covered.

The limited space FT-CPA_{cc} is different compared to the limited space FT-CPA, because the turning manoeuvre for a limited space FT-CPA_{cc} is not limited by the field border (section 2.4.1.5). Therefore, a concave field corner does not have a non-covered area for an FT-CPA.

The path for each swath of the FT-CPA is calculated using a locally oriented, relative coordinate system. Therefore, each path needs to be relocated with respect to the field corner, to place the path in the correct location. This is done by relocating the intersection of the turning manoeuvre (section 2.4.1.7).

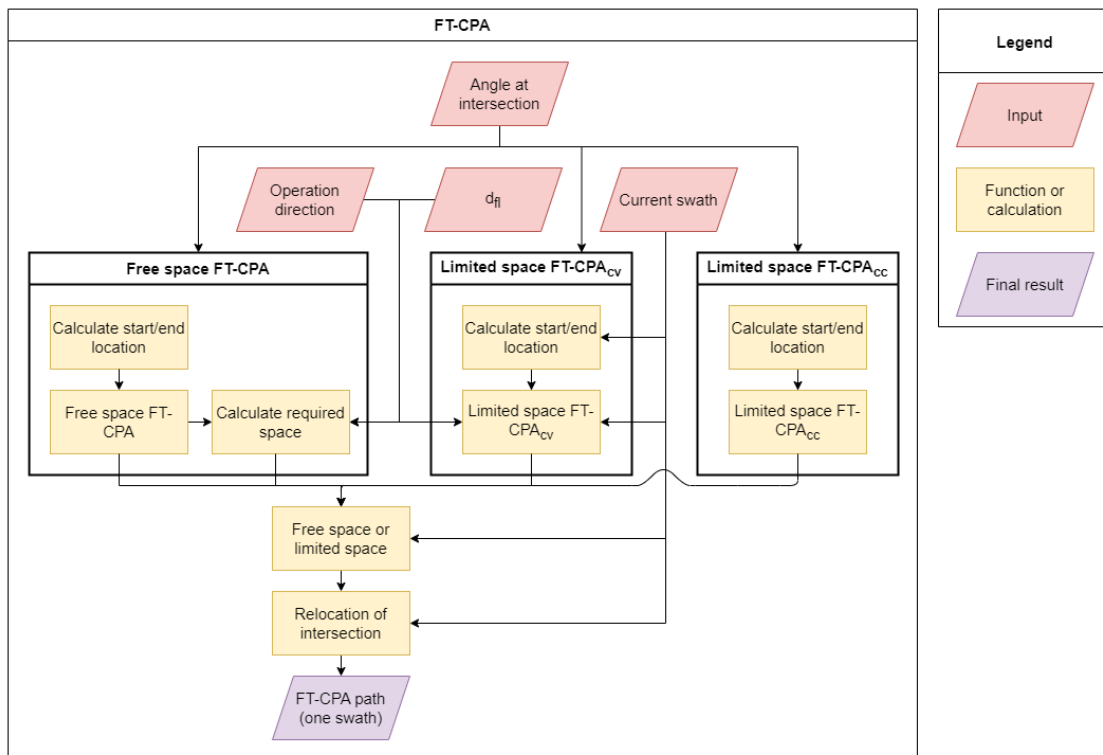


Figure 12: Schematic overview of a FishTail Corner Planning Approach (FT-CPA). Created with DrawIO (2023).

2.4.1.2 Determining start and end location

Each turn operation starts with a start location and ends with an end location. These two locations are important to make a good turn. They are determined by the limiting corner points on the RIC and the width of either the robot, implement, or working area. Furthermore, the start and end location are either determined by the full coverage of the swath (free space FT-CPA and limited space FT-CPA_{cc}), or by the field border (limited space FT-CPA_{cv}). An example is shown in Figure 13.

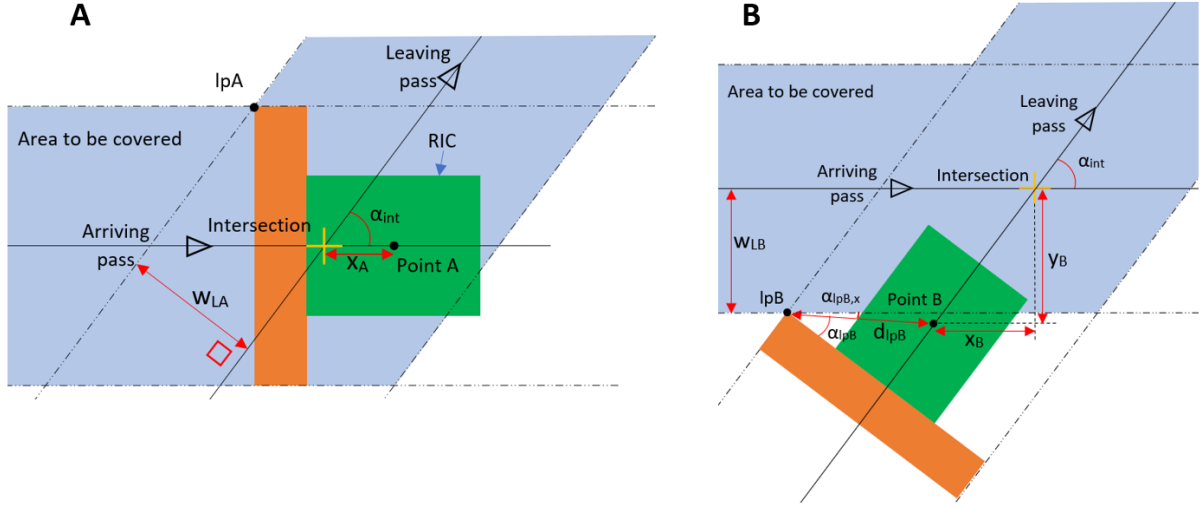


Figure 13: (A) shows how Point A is determined, and (B) shows how Point B is determined. Points A and B are determined by limiting corner points on the RIC and the width of either the robot, implement, or working area. In this figure, the limiting points are determined by full coverage of the swath (blue area) with the working area (orange).

For calculations on the FT-CPA, the origin is set to the intersection between the arriving and leaving pass, the x-axis is set to the arriving pass, the direction of the arriving pass is set to the positive x-axis, and the y-axis is orthogonal to the x-axis. Section 2.4.1.7 explains how the FT-CPA is put into the whole CPA on its corresponding swath. The angle α_{int} in Figure 13 is calculated using Equation 10:

$$\alpha_{int} = \begin{cases} \alpha_{ap} - \alpha_{lp}, & \text{IF } \alpha_{ap} - \alpha_{lp} > 0 \\ \alpha_{ap} - \alpha_{lp} + 2 * \pi, & \text{ELSE} \end{cases} \quad [\text{rad}] \quad (10)$$

where α_{int} is the angle between the arriving pass (α_{ap}) and the leaving pass (α_{lp}), and α_{ap} and α_{lp} are the heading directions of their pass. The north direction is set to 0 and the heading direction can range between 0 and 2π .

The algorithm for calculating the coordinates from Points A and B is detailed in the Appendix in Algorithm A-2.

2.4.1.3 Turning manoeuvre for a free space FishTail Corner Planning Approach

A free space turning manoeuvre is a turn operation that is not constrained by the field border. Therefore, the corner can always be fully covered. The start location Point A and the end location Point B need to be in a location that allows full coverage of the corner. Hence, Point A is determined by the moment when the rear of the working area from the implement is fully within the leaving swath (see Figure 13 (A)). The leaving swath is the area that is covered by the working area from the RIC driving over the leaving pass. Point B is determined by the moment when the front of the working area from the implement is touching the arriving swath (see Figure 13 (B)). However, when the angle α_{int} is between 0 to 0.5π or 1.5π to 2π , the arriving swath until Point A already covered a part of the leaving swath on the side which determines Point B. Therefore, for this range of α_{int} , Point B is not limited by

the arriving pass but by the rear of the working area on Point A. Based on this information, the variables for Algorithm A-2 are determined, which are shown in Table 4.

Table 4: Variable settings for calculating the start and end location for a free space FT-CPA turning manoeuvre.

Angle α_{int}	lpA	lpB	w_{LA}	w_{LB}	F_1
0 to 0.5π	RLW	FLW	y_{FLW}	$y_{FRW} + \cos^2(\alpha_{int}) * w_{work}$	1
0.5π to π	RRW	FRW	y_{FLW}	y_{FRW}	-1
π to 1.5π	RLW	FLW	y_{FRW}	y_{FLW}	1
1.5π to 2π	RRW	FRW	y_{FRW}	$y_{FLW} - \cos^2(\alpha_{int}) * w_{work}$	-1

Now the start and end locations are known, the turning manoeuvre is determined. The turning manoeuvre shown in Figure 14 is used for the free space turning manoeuvre. Figure 14 shows a Reeds-Shepp turn, which looks like a Dubins curve. The main difference is that a Reeds-Shepp turn also allows reverse driving (Reeds & Shepp, 1990). When the RIC has reached Point A, it will start turning around Point C_1 in a forward driving direction. Then, it starts turning around Point C_2 in a backward driving direction. Thereafter it starts turning around Point C_3 in a forward driving direction until it reaches Point B (see Figure 14).

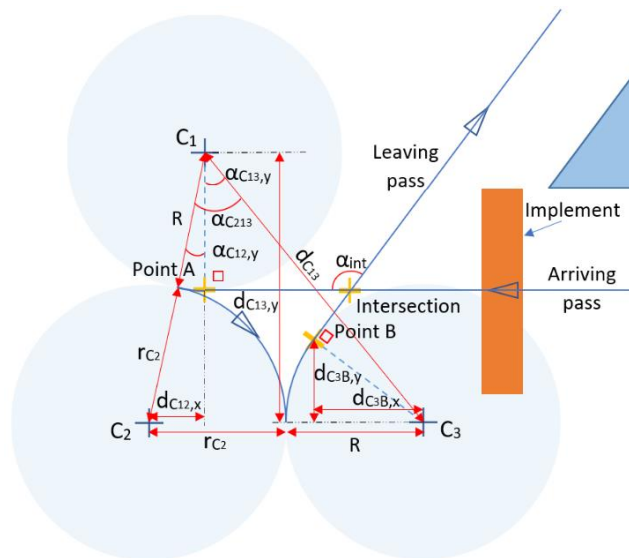


Figure 14: A Reeds-Shepp turn for an FT-CPA. Point A is the point where the implement can be lifted and where the turn operation starts. Point B is the point where the implement needs to be lowered and where the turn operation finishes. This turn is only feasible when the RIC does not cross the field border. The figure shows the dimensions needed to calculate C_1 , C_2 , and C_3 . In the figure, the implement and the working area are the same.

Below, the reasoning for each of the Points C_1 , C_2 , and C_3 are described in more detail.

Point C_1 is located on a line orthogonal to the arriving pass through Point A, and is distanced with the minimum radius R from Point A. Furthermore, it is located on the same side of the arriving pass as the leaving pass is orienting.

Point C_3 is located on a line orthogonal to the leaving pass through Point B, and is distanced with the minimum radius R from Point B. Furthermore, it is located on the opposite side of the leaving pass as the arriving pass is orienting.

Point C_2 is located on the opposite side of the arriving pass as the leaving pass is orienting, and the circle from Point C_2 is intersecting simultaneously the circles from Point C_1 and C_3 . The radius from

the circle from Point C_2 is at least the minimum radius R . However, when Points C_1 and C_3 are too far located from each other, their circles cannot intersect with the circle from Point C_2 . To avoid this non-feasible solution, the radius r_{C_2} from the circle from Point C_2 must be increased to make sure that the circle from Point C_2 intersects with the circles from Point C_1 and C_3 . Additionally, the radius r_{C_2} is iteratively increased by 10% until the length of the path has come to a minimum. Furthermore, Point C_2 is always on a line passing through the centre between C_1 and C_3 and perpendicular to the line connecting C_1 and C_3 .

The calculations for Points C_1 , C_2 , and C_3 are found in Algorithm A-3 in the Appendix. The variable F_2 in Algorithm A-3 equals 1 when α_{int} ranges between 0 and π , while it equals -1 when α_{int} ranges between π and 2π . This is because Point B moves to the opposite side of the arriving pass when $\alpha_{int} = \pi$.

Path of free space FishTail Corner Planning Approach turning manoeuvre

When Points C_1 , C_2 , and C_3 are known, the path for the free space FT-CPA is determined. This was done using Equations 11-13, which calculate a point on a circle with a heading direction:

$$x_{cr} = x_{cc} + \sin(\alpha) * R_{cc} \quad [m] \quad (11)$$

$$y_{cr} = y_{cc} + \cos(\alpha) * R_{cc} \quad [m] \quad (12)$$

$$\alpha_h = \alpha + \frac{1}{2} * \pi * F_0 * F_2 \quad [rad] \quad (13)$$

where (x_{cr}, y_{cr}) is the coordinate for the center of rotation, (x_{cc}, y_{cc}) is the coordinate for the center of the curve, α is the current angle, R_{cc} is the turning radius, F_0 is a factor depending on the forward or backward driving motion of the robot, and F_2 a factor depending on α_{int} .

Using Equations 11-13, the path for the free space FT-CPA can be discretized using a fixed angular step size. The variables needed for every angular step size are found in Table 5 for each circle point.

Table 5: Different values for the variables of Equations 11-13 to calculate the path based on Points C_1 , C_2 , and C_3 for the free space FT-CPA.

Circle point	x_{cc}	y_{cc}	R_{cc}	$\alpha - start$	$\alpha - end$	F_0
C_1	x_{C_1}	y_{C_1}	R	$(1 - F_3) * \pi$	$\alpha_{x_{C_1}y_{C_2}}$	-1
C_2	x_{C_2}	y_{C_2}	r_{C_2}	$-\pi + \alpha_{x_{C_1}y_{C_2}}$	$\alpha_{x_{C_2}y_{C_3}}$	1
C_3	x_{C_3}	y_{C_3}	R	$\alpha_{x_{C_2}y_{C_3}} + \pi$	$\frac{1}{2} * \pi - \alpha_{C_3B,y}$	-1

F_3 is equal to 0 when α_{int} is ranging between 0 and π . F_3 is equal to 1 when α_{int} is ranging between π and 2π .

An example of a free space FT-CPA is shown in Figure 15.

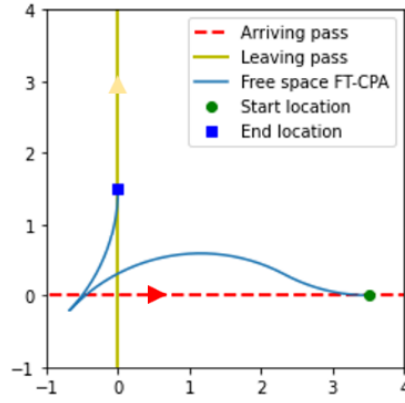


Figure 15: Example of a free space FT-CPA with an angle $\alpha_{int} = 0.5\pi$. The used dimensions for the RIC are found in Table 11, section 3. The RIC is arriving from the west and leaving in the north.

2.4.1.4 Turning manoeuvre for a limited space FishTail Corner Planning Approach at convex corners

In the case of a convex corner, the limited space turning manoeuvre is constrained by the field border. The focus of the limited space FT-CPA_{cv} is that the RIC should never cross the field border, to avoid potentially unwanted collisions. In this study, it is assumed that the field edges near the concerned corner are straight lines. Furthermore, a turn is only possible when there is space left between a RIC on the outer pass and the field border. Fortunately, a no-crop zone around the field border is common due to governmental regulations, because crops located too close to the field border can cause water pollution due to applied chemicals and fertilizers (Steinbusch, 2020). Furthermore, the field border is usually not immediately next to obstacles, allowing some extra space for the hanging implement to cross the field border during the turning manoeuvre. Furthermore, some implements such as sprayers, must not have field border crossing, to avoid potential water pollution (Waterschap Zuiderzeeland, 2019).

This can be achieved using an additional distance between the RIC and the field limit, which is calculated in Equations 14-15:

$$d_{ifl} = d_{ncz} + d_{extra} \quad [m] \quad (14)$$

$$d_{rfl} = d_{ncz} \quad [m] \quad (15)$$

where d_{ifl} is the distance between the implement and the field limit, d_{ncz} is the distance for the no-crop zone, d_{extra} is the distance an implement can cross the field border, and d_{rfl} is the distance between the robot and the field limit. d_{rfl} is different compared to d_{ifl} , because the robot may not leave the field border, because the field border could be next to a ditch. With these two different distances, the robot is allowed to drive over the no-crop zone, but cannot cross the field border. An example of the field limit with a limited space FT-CPA_{cv} is shown in Figure 16.

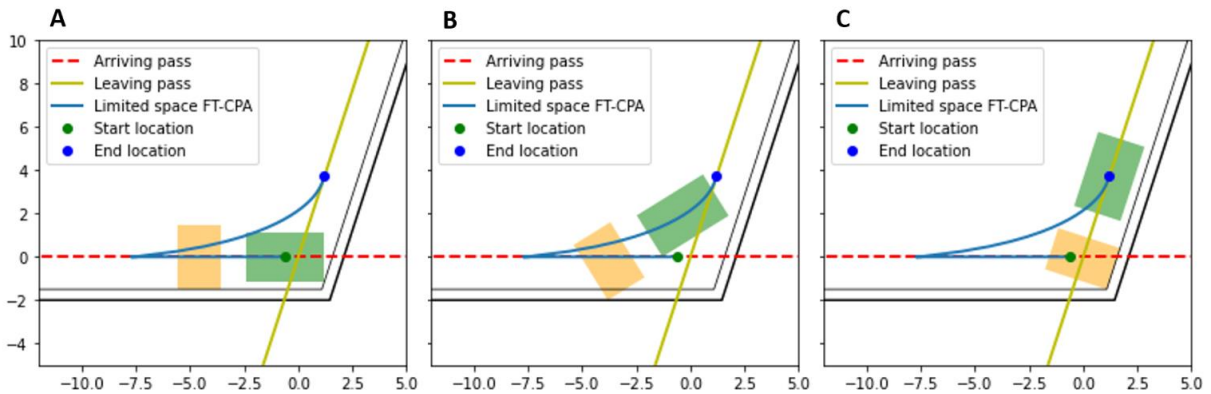


Figure 16: Example of a limited space FT-CPA_{cv}. (A) shows the start position, (B) shows an intermediate position, and (C) shows the end position of a limited space FT-CPA_{cv}. The thin black line is the field border and the thick black line is the field limit. During the turning manoeuvre (B), the implement does not cross the field limit.

Determine the start and end location for a limited space FishTail Corner Planning Approach at convex corners

The first aspect needed for obtaining the limited space turning manoeuvre is to determine the start and end location of the turning manoeuvre. An example of determining the start and end location is shown in Figure 13. These locations are determined using Algorithm A-2 in the Appendix. Because the limited space turning manoeuvre is limited by the field border, the start location is determined by either the front side of the robot or the implement, depending on the angle α_{int} and the dimensions from the RIC. The end location is either determined by the rear of the implement or the robot.

As can be seen in Figure 11, the limited space FT-CPA_{cv} could also be used for a second or higher closest pass to the field border. In these situations, the limited space FT-CPA_{cv} uses the extra space from the other swaths to allow a higher coverage of the corner. Therefore, the algorithm needs as input the number of passes that can be driven over. Based on these limitations, the values for Algorithm A-2 are determined, which are found in Table 6.

Table 6: Variable settings for calculating the start and end location for a limited space FT-CPA_{cv} turning manoeuvre. lpA-robot and lpB-robot are the limiting points of the robot, and lpA-im and lpB-im are the limiting points of the implement. N_{ap} and N_{lp} are the number of passes that can be driven over next to the arriving and leaving pass, consecutively.

Angle α_{int}	lpA-robot	lpB-robot	lpA-im	lpB-im	w_{LA}	w_{LB}	F_1
0 to 0.5π	FRR	RRR	FRI	RRI	$y_{FRI} - N_{lp} * w_{work}$	$y_{FRI} - N_{ap} * w_{work}$	-1
0.5π to π	FLR	RLR	FLI	RLI	$y_{FRI} - N_{lp} * w_{work}$	$y_{FRI} - N_{ap} * w_{work}$	1
π to 1.5π	FRR	RRR	FRI	RRI	$y_{FLI} + N_{lp} * w_{work}$	$y_{FLI} + N_{ap} * w_{work}$	-1
1.5π to 2π	FLR	RLR	FLI	RLI	$y_{FLI} + N_{lp} * w_{work}$	$y_{FLI} + N_{ap} * w_{work}$	1

The coordinates of Points A and B are both calculated for a limiting robot and implement. However, only one point on the RIC can limit Points A or B. Therefore, the right point needs to be selected from the two options from either the robot or the implement. Furthermore, when there are passes that can be driven over, the RIC might drive further than needed with the variable settings from Table 6 to cover the corner. Therefore, the start and end location from the free space turning manoeuvre should also be considered (Table 4), to avoid unnecessary driving. This will end up in three possible locations for Points A and B. To get the right location for Points A and B, Algorithm 2 is used:

Algorithm 2: Points A and B for a limited space FT-CPA_{cv}

$$x_A = \min(x_{A-robot}, x_{A-im}, x_{A-freespace})$$

IF $0 < \alpha_{int} < \pi$ **THEN:**

$$y_B = \max(y_{B-robot}, y_{B-im}, y_{B-freespace})$$

IF $\pi < \alpha_{int} < 2 * \pi$ **THEN:**

$$y_B = \min(y_{B-robot}, y_{B-im}, y_{B-freespace})$$

$$x_B = \frac{y_B}{\tan(\alpha_{int})}$$

An example of a start and end location of a limited space FT-CPA_{cv} is shown in Figure 16 (A) and (C).

Determine the limiting point on the RIC during turning

Once the start and end locations are known for the limited space FT-CPA_{cv}, the turning manoeuvre is to be determined. Driving close to the field border and making a turn operation with a fixed turning radius might result in a point on the RIC crossing the field border, which is undesired. To avoid crossing the field border, the limiting point on the RIC prone to crossing the field border needs to be found. This limiting point depends on the position of the implement and the dimensions of the RIC. This limiting point is either at the rear of the robot or the rear of the implement. The corner points on the rear of the robot and implement which are closest to the field border are the potential limiting points.

Points in front of the center of rotation of the RIC are never limiting because these move away from the field border during a turning manoeuvre. Hence, the limiting point is the point on the RIC which is most remote from the center of the curve and behind the center of rotation. Based on these characteristics, the limiting point is determined, as detailed in Algorithm A-4 in the Appendix.

Calculating the path of the turning manoeuvre for a limited space FishTail Corner Planning Approach at convex corners

When the limiting point is known for the limited space FT-CPA_{cv} turning manoeuvre, the path of the turning manoeuvre is calculated. The full turning path can consist of three Parts: the Part 1 is limited by R , the Part 2 is limited by the limiting point on the RIC, and Part 3 is limited again by R . This is visualised in Figure 17. The path does not have to consist of the three different Parts. This depends on all the dimensions and the angle α_{int} . When the limiting point on the RIC from Part 2 never touches the field limit, it will not limit the turn operation and therefore only Part 1 is limiting the turning manoeuvre.

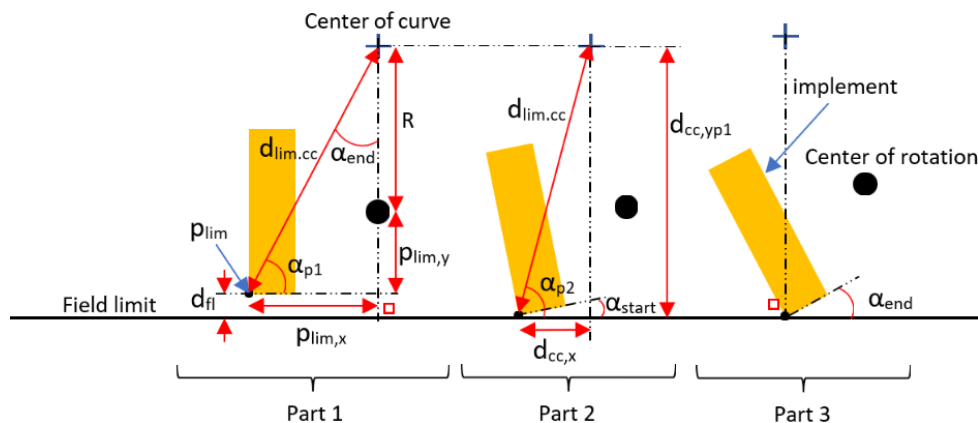


Figure 17: The path for a limited space FT-CPA_{cv} turning manoeuvre can consist of three Parts, which are either determined by the R or the limiting point on the RIC. The field limit is a line parallel to the field border with an offset d_{fi} .

All the angles and distances shown in Figure 17 are calculated using Algorithm A-5 in the Appendix. Depending on these angles and distances, not all the Parts might be required. In Algorithm 3, the required Parts for making the limited space FT-CPA_{cv} turning manoeuvre are determined, together with the angle range for each Part.

Algorithm 3: Determining required Parts for a limited space FT-CPA _{cv} turning manoeuvre	
Calculate the needed angle at the intersection	Explanation
IF $\alpha_{int} > \pi$ THEN: $\alpha_{int2} = 2 * \pi - \alpha_{int}$ ELSE: $\alpha_{int2} = \alpha_{int}$	When α_{int} is larger than π , the whole FT-CPA turns to the other side of the arriving pass. Therefore, the angle on the other side of the intersection is needed. The angle α_{int2} is ranging between 0 and π .

Selecting the required Parts	
IF $d_{cc,yp1} > d_{lim,cc}$ OR $\alpha_{start} > \alpha_{int2}$ THEN: Only Part 1 is required. α_{hp1} is ranging from 0 to α_{int2}	when $d_{cc,yp1} < d_{lim,cc}$, the limiting point on the RIC will never touch the field limit. When $\alpha_{start} > \alpha_{int2}$, the heading direction for the leaving pass is in the range of Part 1.
ELSEIF $\alpha_{end} > \alpha_{int2}$ THEN: Parts 1 and 2 are required. α_{hp1} is ranging from 0 to α_{start} α_{hp2} is ranging from α_{start} to α_{int2}	When $\alpha_{end} > \alpha_{int2}$, the heading direction for the leaving pass is in the range of Part 2.
ELSE: Parts 1, 2, and 3 are required. α_{hp1} is ranging from 0 to α_{start} α_{hp2} is ranging from α_{start} to α_{end} α_{hp3} is ranging from α_{end} to α_{int2}	The heading direction for the leaving pass is in the range of Part 3.

For calculating the path from Parts 1-3, the origin is set to the center of rotation at the start of Part 1, the x-axis is the arriving pass, and the y-axis is orthogonal to the x-axis. The path for Part 1 is calculated using Equations 16-18, using the range determined according to Algorithm 3:

$$x_{crp1} = R * \sin(\alpha_{hp1}) \quad [m] \quad (16)$$

$$y_{crp1} = F_2 * R * (1 - \cos(\alpha_{hp1})) \quad [m] \quad (17)$$

$$a_h = \frac{1}{2}\pi - F_2 * a_{hp1} \quad [rad] \quad (18)$$

In Part 2, the turning radius R does not longer hold because otherwise the field limit is crossed by the limiting point. Therefore, the path in Part 2 is no longer determined by a fixed turning radius, but by the limiting point on the RIC. To allow the fastest turning possible in Part 2, the turning radius should be as low as possible. Therefore, the limiting point should always touch the field limit, which is only possible when the center of the curve is always above the limiting point during Part 2 (see Figure 18). Furthermore, the center of rotation cannot experience a lateral shift due to mechanical constraints. Therefore, the angle between the driving direction and the center of the curve should always be orthogonal.

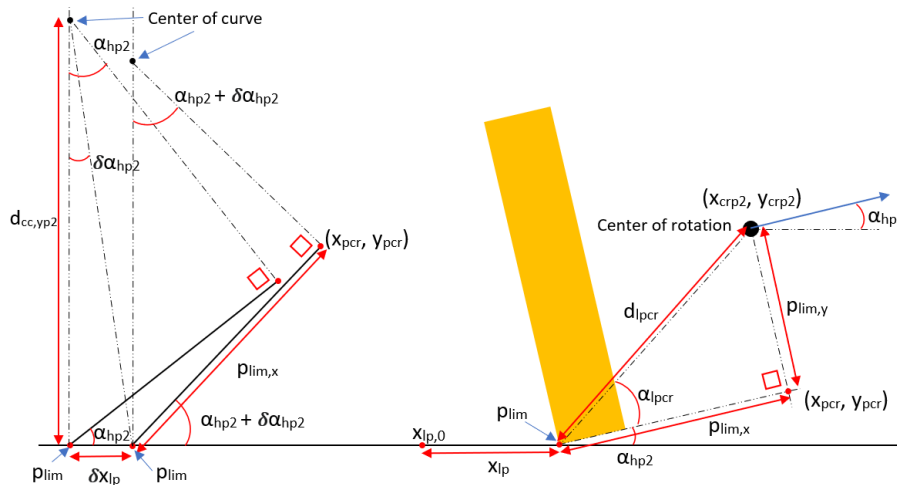


Figure 18: The needed dimensions to calculate the path for the center of rotation for Part 2 from the limited space FT-CPA_{cv} turning manoeuvre. The figure on the left shows the needed dimensions to calculate the location of the limiting point from

the RIC for a varying angle α_{hp2} . The figure on the right shows the needed dimensions to calculate the location from the center of rotation.

Because in Part 2 the path is determined by the limiting point on the RIC, the path for the center of rotation should be expressed using the path from this limiting point. The limiting point should always touch the field border. Therefore, the path of the limiting point only needs to be determined for the x-axis, which is expressed using the angle α_{hp2} . Because this equation cannot be directly obtained, the path of the limiting point on the x-axis is described by the rate of change using Equation 19:

$$\delta x_{lp}(\alpha_{hp2}) = d_{cc,yp2} * \tan(\delta\alpha_{hp2}) = \frac{p_{lim,x}}{\sin(\alpha_{hp2})} * \tan(\delta\alpha_{hp2}) \quad [m] \quad (19)$$

This is shown in Figure 18. Furthermore, Equation 20 also holds:

$$\lim_{x \rightarrow 0} \left(\frac{\tan(x)}{x} \right) = 1 \quad [-] \quad (20)$$

When Equations 19 and 20 are combined, the part $\tan(\delta\alpha_{hp2})$ in Equation 19 can be substituted by $\delta\alpha_{hp2}$, as long as $\delta\alpha_{hp2}$ is close to zero. Fortunately, this is possible when Equation 19 is integrated. Furthermore, now the part $\tan(\delta\alpha_{hp2})$ from Equation 19 is substituted with $\delta\alpha_{hp2}$, Equation 19 is integrated to obtain the position of x_{lp} for an angle α_{hp2} , with an initial angle α_{start} . This results in the following integral (Equation 21):

$$x_{lp}(\alpha_{hp2}) = \int_{\alpha_{start}}^{\alpha_{hp2}} \frac{p_{lim,x}}{\sin(\alpha)} \delta\alpha \quad [m] \quad (21)$$

The integration of Equation 21 was solved using Mathway (2022), yielding Equation 22:

$$x_{lp}(\alpha_{hp2}) = p_{lim,x} * \ln \left| \frac{\sin(\alpha_{start}) * (\cos(\alpha_{hp2}) - 1)}{\sin(\alpha_{hp2}) * (\cos(\alpha_{start}) - 1)} \right| + x_{lp,0} \quad [m] \quad (22)$$

where $x_{lp,0} = -d_{cc,x}$. Equation 22 describes the path of the limiting point from the RIC. Based on this path, the path from the center of rotation is calculated, which is done using Equations 23-25:

$$x_{crp2} = x_{lp}(\alpha_{hp2}) + d_{lpcr} * \cos(\alpha_{hp2} + \alpha_{lpcr}) \quad [m] \quad (23)$$

$$y_{crp2} = F_2 * (d_{lpcr} * \sin(\alpha_{hp2} + \alpha_{lpcr}) - p_{lim,y} - d_{fl}) \quad [m] \quad (24)$$

$$a_h = \frac{1}{2}\pi - F_2 * a_{hp2} \quad [rad] \quad (25)$$

Where the angles and dimensions used are shown in Figure 18 and are calculated using Algorithm A-6 in the appendix.

The path for Part 3 is calculated using Equations 26-28, which is similar to the calculations of the path in Part 1 (Equations 16-18):

$$x_{crp3} = x_{lp}(\alpha_{end}) + R * \sin(\alpha_{hp3}) \quad [m] \quad (26)$$

$$y_{crp3} = F_2 * (d_{lim,cc} - d_{cc,yp1} + R * (1 - \cos(\alpha_{hp3}))) \quad [m] \quad (27)$$

$$a_h = \frac{1}{2}\pi - F_2 * a_{hp3} \quad [rad] \quad (28)$$

The coordinate system of Parts 1-3 uses the start point of Part 1 as the origin. However, the required coordinate system of the limited space FT-CPA_{cv} uses the intersection between the arriving and leaving pass as the origin. The difference between the coordinate systems concerns a shift of the origin on the

x-axis. To calculate this shift, the end location of the path of Parts 1-3 ($x_{cr,end}, y_{cr,end}$) and the angle α_{int} are required, which is done using Equation 29:

$$x_{shift} = -x_{cr,end} + \frac{y_{cr,end}}{\tan(\alpha_{int})} \quad [m] \quad (29)$$

This shift for the x coordinates needs to be added to the path from Parts 1-3. By adding this shift, the origin of the path is at the intersection between the arriving and leaving pass, leading to the required coordinate system of the limited space FT-CPA_{cv}.

2.4.1.5 Turning manoeuvre for a limited space FishTail Corner Planning Approach at a concave corner

The shortest path to connect the arriving and leaving pass at a corner is to use the free space FT-CPA. However, also at a concave corner, the free space FT-CPA requires minimum space for the turning manoeuvre. Therefore, a limited space FT-CPA is required that takes the field border into account. However, the limited space FT-CPA_{cv} of section 2.4.1.4 is determined for a convex corner and therefore may produce infeasible solutions for concave corners. Hence, a different limited space FT-CPA is required for concave corners (limited space FT-CPA_{cc}). The focus of the limited space FT-CPA_{cc} is that the RIC should never cross the field border, to avoid potentially unwanted collisions. The main difference between the limited space FT-CPA_{cv} and FT-CPA_{cc} is that the turning manoeuvre for the limited space FT-CPA_{cc} is planned on the other side of the intersection compared to the limited space FT-CPA_{cv} (Figure 19). Therefore, the limited space FT-CPA_{cc} never crosses the field border at concave corners.

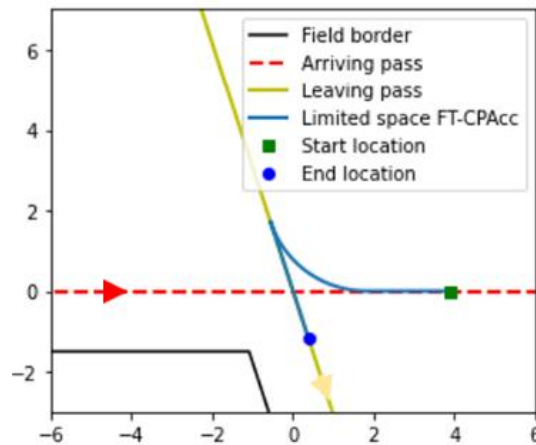


Figure 19: Example of a limited space FT-CPA_{cc}. When the RIC is driving over the path, it will never cross the field border. The RIC is arriving from the west and leaving to the south.

The limited space FT-CPA_{cc} connects the arriving and leaving pass with a single circular turning manoeuvre with the radius R . The center of the curve of the turning manoeuvre is always on the opposite side of the intersection with respect to the field corner, see Figure 19. Furthermore, because the limited space FT-CPA_{cc} is not limited by the field border, the start and end locations from the free space FT-CPA are used as start and end locations for the limited space FT-CPA_{cc}. With these criteria, the limited space FT-CPA_{cc} is determined, which is found in Algorithm A-7 in the Appendix.

2.4.1.6 Feasibility of free space FishTail Corner Planning Approach

The next step in creating an FT-CPA is to determine the minimum space required for the free space FT-CPA. In a free space FT-CPA, the RIC must not exceed the field limits. Therefore, it is important to determine how much space is required for making the turning manoeuvre. Based on this minimum required space, the minimum number of swaths between the current swath and the field border is calculated (N_{ap} for the arriving pass, and N_{lp} for the leaving pass).

To calculate the minimum required space, the locations of all the corner points from the RIC are needed for the whole turning manoeuvre. Therefore, the paths for the corner points from the RIC are calculated based on the path of the center of rotation. These paths are calculated using Equations 30-31:

$$x_{pathcp} = x_{cr} + x_{cp} * \sin(\alpha_h) - y_{cp} * \cos(\alpha_h) \quad [m] \quad (30)$$

$$y_{pathcp} = y_{cr} + y_{cp} * \sin(\alpha_h) + x_{cp} * \cos(\alpha_h) \quad [m] \quad (31)$$

Where (x_{pathcp}, y_{pathcp}) is a point on the path of the corner point and (x_{cp}, y_{cp}) are the coordinates of the corner point on the RIC (Table 1).

A corner can be divided into two areas; an area that is closer to the arriving pass, and an area that is closer to the leaving pass (Figure 20). Therefore, each point on the path of a corner point can be either in the area closer to the arriving pass or the leaving pass. Furthermore, only the points which are potentially limiting should be selected to determine the minimum required space. These potentially limiting points are only between the pass and the field border, see Figure 20. For all these points, the distance to the pass is calculated. The highest distance between the points and each pass determines the minimum space required for each pass.

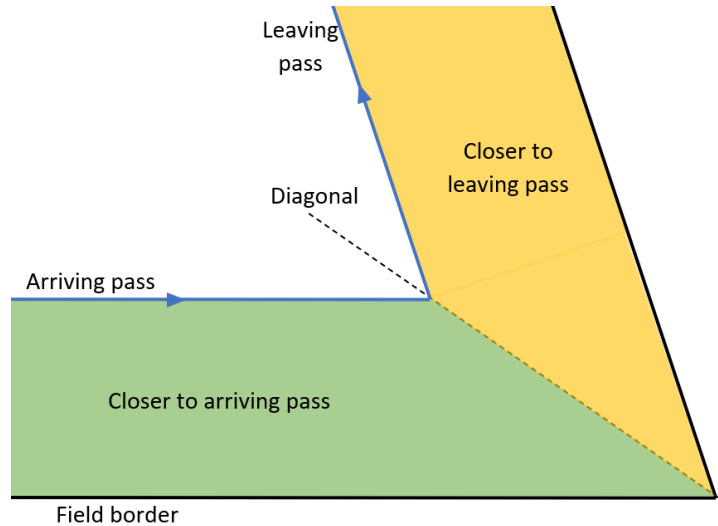


Figure 20: The area between the arriving or leaving pass and the field border is split up into two parts. Closer to the arriving pass or closer to the leaving pass.

The found distances describe the minimum distance needed between the arriving or leaving pass and the field border. To find the numbers for N_{ap} and N_{lp} , the distances need to be corrected for the machine width and the permitted exceedance of the field border. These two corrections depend on the operation direction of the field (clockwise or counter-clockwise) and the distances d_{ifl} and d_{rfl} . For a clockwise operation direction, the left side of the RIC is limiting, for a counter-clockwise operation direction, the right side of the RIC is limiting. To correct for the machine width, the distance between the pass and the limiting side (left or right) must be subtracted from the minimum distance needed. Furthermore, the distance d_{ifl} or d_{rfl} also need to be subtracted, depending on if the machine is the implement or the robot.

Because the distances d_{ifl} and d_{rfl} do not have to be equal, the distance between the arriving and leaving pass and the field border need to be determined for the robot and implement separately. Besides the four corner points of the robot (FLR, FRR, RLR, RRR), the points next to the center of rotation also need to be used. The coordinates of these two points are $(0, 0.5 * w_{robot})$ and $(0, -0.5 * w_{robot})$.

w_{robot}). These two points are also needed because they are the closest points on the robot to the center of the curve and might therefore need more space during a turning manoeuvre compared to the other corner points. For the implement the corner points FLI, FRI, RLI, and RRI are used.

When the remained minimum distances required for each pass for the robot and implement are known, the highest minimum distance for each pass is selected (from the robot or the implement). These two distances are divided by the working width and rounded up, resulting in the numbers for N_{ap} and N_{lp} .

2.4.1.7 Relocation of intersection for a FishTail Corner Planning Approach

When a path is created for an FT-CPA, the x-axis is used as the arriving pass. However, a field corner normally has several swaths which must be covered. Therefore, the path for each swath must be relocated to place it on its corresponding swath. In this new coordinate system, the field corner is set to the origin, and the field border parallel to the arriving swaths is the x-axis. In the local coordinate system from a path the intersection between the arriving and leaving pass is the origin. However, in the new coordinate system, this intersection is relocated to its corresponding swath. This change in the coordinate system is applied to the whole path from the local coordinate system to put the whole turning manoeuvre in the right position relative to the field corner.

To obtain the location of the intersection in the new coordinate system the operation direction of the path planning is required. For a clockwise direction, the left side of the RIC is facing the field border. For a counter-clockwise direction, the right side of the RIC is facing the field border. Based on the operation direction and the current swath number, the distance is calculated between the current swath and the field border. Using this distance, the arriving and leaving pass are determined. Next, the intersection between the arriving and leaving pass is determined using the Python library SymPy (2021). The coordinates of this intersection are used to relocate the path for the turning manoeuvre relative to the field corner.

2.4.2 Continuous Corner Planning Approach

Not all field corners are sharp. This is especially the case for irregular field shapes. If corners with obtuse angles are planned with an FT-CPA, some area is lost for the turning manoeuvres. Therefore, it might be better to continue driving in these corners, without turning. In this study, this is called the Continuous Corner Planning Approach (C-CPA). The advantages of this C-CPA are that the operation time is decreased and there is less soil compaction. A disadvantage is that not every part of the corner is covered because the turning requires some space. Furthermore, the turning radius of the C-CPA is larger than the R , because the implement still needs to do its work. The minimum turning radius for a RIC with an implement at work (R_w) can be determined by several factors. In this study, the R_w is determined by the minimum effective working width required, which is a percentage of the real working width. Because the implement is not located in the center of rotation, the effective working width will become smaller due to the curve (see Figure 21).

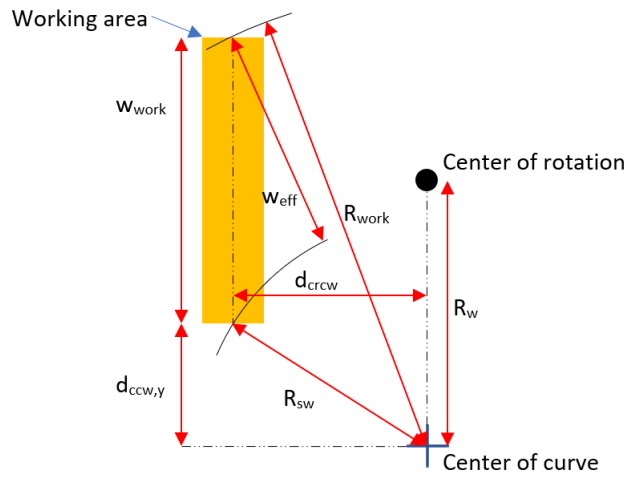


Figure 21: The effective working width (w_{eff}) changes with a varying R_w .

When the working area has an offset, the R_w differs between a left and a right turn. To avoid this difference, the R_w is determined for the middle of the side of the working area (R_{sw}) closest to the center of curve. This value is equal for either a left or a right turn. The R_{sw} is based on Equation 32:

$$R_{sw} = R_{work} - w_{eff} \quad [m] \quad (32)$$

The calculation for R_{sw} is found in Algorithm A-8 in the Appendix.

2.4.2.1 Calculate the rotation points for a Continuous Corner Planning Approach

Continuous corner planning needs somewhat different approaches for convex and concave corners (Figure 22). Based on the radius R_{sw} , a new field border is created. For creating a C-CPA, the new field border should always be within the original field to avoid crossing the field border (see Figure 22). Furthermore, the radius for a side of the working area cannot be smaller than R_{sw} for any pass on the headland. Therefore, for a convex corner, the side of the working area at the inner field border has the radius R_{sw} , see Figure 22 (B). The point C_{cv} from Figure 22 (B) is distanced equally from each side of the corner. This distance is the minimum radius R_{sw} plus the headland width w_{hl} .

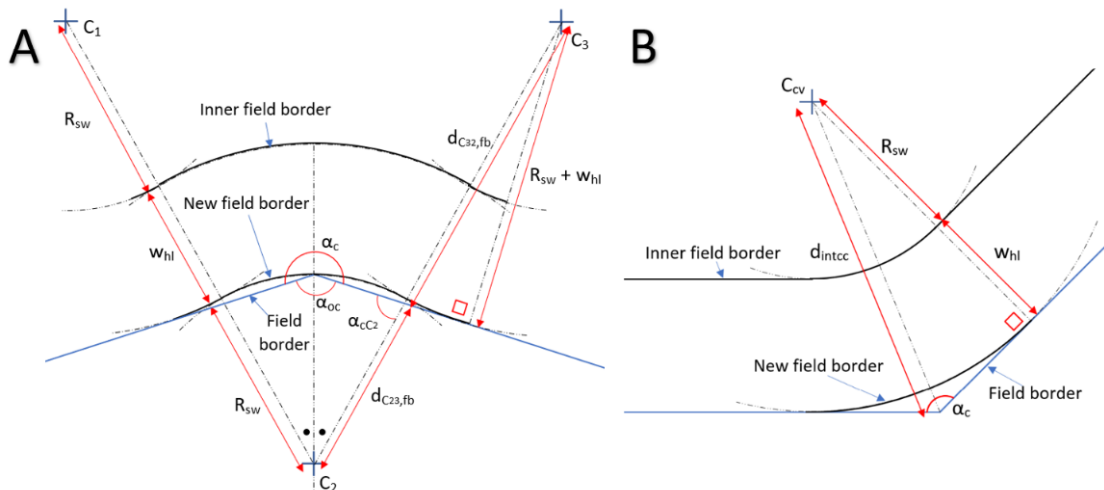


Figure 22: Continuous turning in a concave corner (A) and a convex corner (B). Both figures show the needed dimensions to calculate the new field border for a C-CPA.

For a concave corner, the angle between the new field border and the original field border at the corner is equal for the left and the right side of the corner, see Figure 22 (A). Furthermore, the new

field border is going through the original corner, and the start and end points of the new field border are located on the original field border.

Based on these constraints, the locations of C_1, C_2, C_3 , and C_{cv} are calculated. For these calculations, the origin is set to the corner, the x-axis is set to the arriving edge from the field border, and the y-axis is orthogonal to the x-axis. These calculations are shown in Algorithm A-9 in the Appendix.

When the locations of C_1, C_2, C_3 , and C_{cv} are known, the new field border is calculated using Equations 11-13 and the variables from Table 7.

Table 7: Different values for the variables of Equations 11-13 to calculate the new field border based on Points C_1, C_2, C_3 , and C_{cv} for the C-CPA.

CIRCLE POINT	x_{cc}	y_{cc}	R_{cc}	$\alpha - start$	$\alpha - end$	F_o
C_1	x_{C_1}	y_{C_1}	$R_{sw} + w_{hl}$	π	$\frac{1}{2} * \pi + \alpha_{cc2}$	-1
C_2	x_{C_2}	y_{C_2}	R_{sw}	$-\frac{1}{2} * \pi + \alpha_{cc2}$	$1\frac{1}{2} * \pi - \alpha_{cc2} - \alpha_{oc}$	1
C_3	x_{C_3}	y_{C_3}	$R_{sw} + w_{hl}$	$2\frac{1}{2} * \pi - \alpha_{cc2} - \alpha_{oc}$	α_c	-1
C_{cv}	x_{cc}	y_{cc}	$R_{sw} + w_{hl}$	π	α_c	-1

2.4.2.2 Calculate the path for a Continuous Corner Planning Approach

With the known locations for the circle points, the path for each swath at the corner is calculated. This path uses the same values shown in Table 7, except for the turning radius R_{cc} . The radius depends on the current swath number and the field operation direction. In Table 8, the required radiuses at each different swath number are determined. Combining these radiuses with Table 7 and Equations 11-13 results in the paths for each different swath of a C-CPA.

Table 8: Required radiuses for calculating a path of a C-CPA, where N_{swath} is the current swath number, which is counted from the inner field border to the field border.

Circle point	R_{cc} clockwise direction	R_{cc} counter-clockwise direction
C_1	$R_{sw} - y_{FRW} + (N_{swath} - 1) * w_{work}$	$R_{sw} + y_{FLW} + (N_{swath} - 1) * w_{work}$
C_2	$R_{sw} + w_{hl} + y_{FRW} - (N_{swath} - 1) * w_{work}$	$R_{sw} + w_{hl} - y_{FLW} - (N_{swath} - 1) * w_{work}$
C_3	$R_{sw} - y_{FRW} + (N_{swath} - 1) * w_{work}$	$R_{sw} + y_{FLW} + (N_{swath} - 1) * w_{work}$
C_{cv}	$R_{sw} - y_{FRW} + (N_{swath} - 1) * w_{work}$	$R_{sw} + y_{FLW} + (N_{swath} - 1) * w_{work}$

2.4.2.3 Correction for corner orientation

Depending on the operation direction (clockwise or counter-clockwise), the field border is either on the left or the right side. However, the C-CPA is calculated using a simplified orientation with the field border always on the right side. To correct for this orientation, all the y coordinates must be multiplied with -1 when $\alpha_{int} > \pi$. Because of this correction, the heading direction must also be multiplied by -1, and a value of π must be added to the heading directions. With these corrections, the C-CPA has the right coordinates with its corresponding heading direction.

2.4.3 Calculate the non-covered area of a turning manoeuvre

During a turning manoeuvre, it is not always possible to cover the whole area because the field border limits the RIC in covering the whole area. The CPA is optimised by minimizing the non-covered area. Each different type of turning manoeuvre has its own calculation of the non-covered area. In this

section, the non-covered area is determined for the FT-CPA and the C-CPA. The library from Shapely (2022) in Python is used to calculate the non-covered area.

2.4.3.1 Non-covered area for a FishTail Corner Planning Approach

The non-covered area for a free space FT-CPA or a limited space FT-CPA_{cc} is always zero, but for a limited space FT-CPA_{cv} there is always a non-covered area. The non-covered area for an FT-CPA is determined by the start location Point A and the end location Point B. The non-covered area is determined as the area which is not fully covered by the whole working area. Therefore, the non-covered area of the arriving pass is determined by the rear of the working area at Point A. The non-covered area of the leaving pass is determined by the front of the working area at Point B. An example is shown in Figure 23.

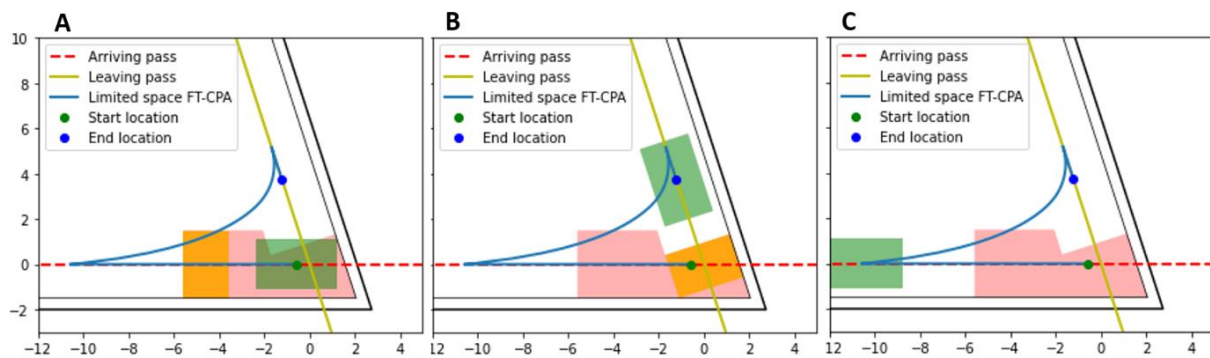


Figure 23: Example of a non-covered area from a limited space FT-CPA_{cv}. (A) shows the situation at the start location on Point A where the rear of the working area determines a side from the non-covered area. (B) shows the situation at the end location on Point B where the front of the working area determines a side from the non-covered area, and (C) shows the non-covered area in red.

To find the non-covered area, the area that should be covered by the arriving and leaving swath is determined first. Secondly, the area which is covered by the arriving swath and leaving swath is determined. Thirdly, the latter is subtracted from the area that should be covered by the arriving and leaving swath using the function difference from Shapely. This results in the non-covered area.

2.4.3.2 Non-covered area for a Continuous Corner Planning Approach

The non-covered area for a C-CPA was calculated using the new field border determined in section 2.4.2. The area between the new field border and the original field border is determined using Shapely.

2.4.4 Choose the optimal Corner Planning Approach

In this study, there are two options for corner planning; the FT-CPA and the C-CPA. The optimal CPA is determined using the non-covered area and the driven distance to cover the field corner. This is done for all the swaths in the corner. Because the turning manoeuvre from the C-CPA requires more space, the start and end locations are added to the paths from the FT-CPA, to make sure that both turning manoeuvres have the same start and end locations. The non-covered area and the driven distance differ between the FT-CPA and C-CPA and change with a varying angle at the field corner. Therefore, depending on the angle, either the FT-CPA or the C-CPA is optimal. In Figure 24, an example is shown between a corner planned using the C-CPA and the FT-CPA.

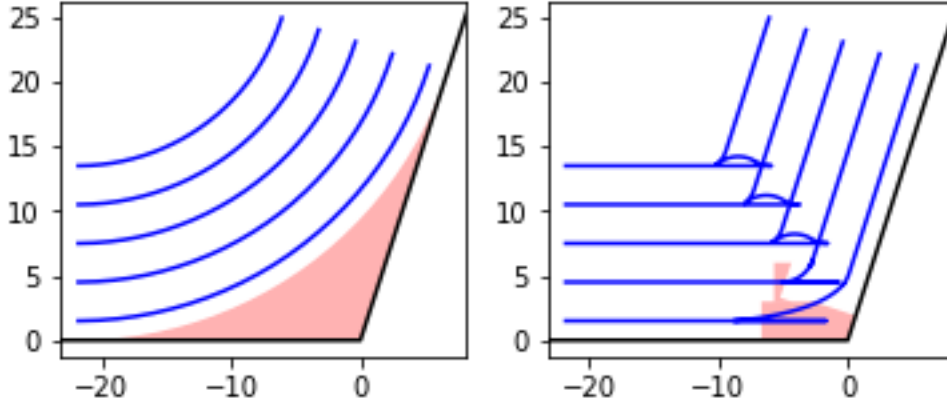


Figure 24: Example of a C-CPA (left) and an FT-CPA (right) for an equally angled corner. The blue lines are the paths for each different swath. The start and end locations for each swath between the C-CPA and the FT-CPA are equal. The red area is the non-covered area. In this figure, the FT-CPA is better compared to the C-CPA.

The optimal CPA is determined using Equation 33, which uses the relative difference between the sum of two values and the difference between those two values:

$$f_{obj} = \frac{nca_C - nca_{FT}}{nca_C + nca_{FT}} + \frac{d_C - d_{FT}}{d_C + d_{FT}} \quad [-] \quad (33)$$

where f_{obj} is the outcome of the objective function, nca_C is the non-covered area from the C-CPA, nca_{FT} is the non-covered area from the FT-CPA, d_C is the travelled distance from the C-CPA, and d_{FT} is the travelled distance from the FT-CPA. When the value from f_{obj} is less than 0, the C-CPA is optimal. When it is higher than 0, the FT-CPA is optimal.

However, the non-covered area from an FT-CPA at a concave corner is always 0, because the start and end locations are not limited by the field border. This would result in having always an FT-CPA at concave corners. Even at corners where the heading direction barely changes and a C-CPA would be better. To avoid this problem, a threshold was set to the non-covered area of the FT-CPA at a concave corner. This threshold is determined by using the non-covered area from an FT-CPA at an orthogonal corner angle.

A better solution instead of the threshold is to expand the objective function. Another good indicator for judging a CPA is using the area the tracks/wheels of the RIC require of just covered parts from the field because it is unwanted to drive over freshly tilled soil or seeded areas. However, this did not fit within the scheduled time for this study and is therefore left for future work.

2.4.5 Reprojection of the Corner Planning Approach

For the calculation of the CPAs, the corner location and orientation were projected to a locally oriented reference system. This system needs to be reprojected, to include it in the original field CPP. This reprojection is performed using Equations 34-35, which are adapted equations from the Department of Mathematics (2022).

$$x_{field} = x_c + x_{loc} * \cos\left(\alpha_{ap} - \frac{1}{2} * \pi\right) + y_{loc} * \sin\left(\alpha_{ap} - \frac{1}{2} * \pi\right) \quad [m] \quad (34)$$

$$y_{field} = y_c - x_{loc} * \sin\left(\alpha_{ap} - \frac{1}{2} * \pi\right) + y_{loc} * \cos\left(\alpha_{ap} - \frac{1}{2} * \pi\right) \quad [m] \quad (35)$$

where (x_{loc}, y_{loc}) are the coordinates from the local orientation, (x_c, y_c) is the coordinate from the field corner, and (x_{field}, y_{field}) is the final coordinate of the point in the original field.

2.5 Headland Coverage Path Planning

For creating the headland CPP, the optimal CPAs for each corner are needed. The optimal CPA is determined using the objective function in section 2.4.4. Given the optimal CPAs for each corner, the headland CPP is created. In this study, the headland CPP has a spiral pattern, see Figure 25. Furthermore, the CPP also requires a start and an end location. A field operation normally starts and ends in a field corner. Therefore, a field corner must be selected which is used as a start corner. This start corner is normally the closest field corner to the field entry location.

Moreover, for the creation of the headland CPP, also the field operation direction and the start border are required. The start border is either at the inner field border or the field border, depending on the type of field operation. A seeding or cultivating operation normally starts at the inner field border, to avoid driving over already covered areas. A harvesting operation normally starts at the field border, to avoid driving over non-harvested areas.

With all this information, the headland CPP is planned in the correct order. Section 2.5.1 explains how the start and finish locations are determined. Section 2.5.2 explains how the headland CPP is determined.

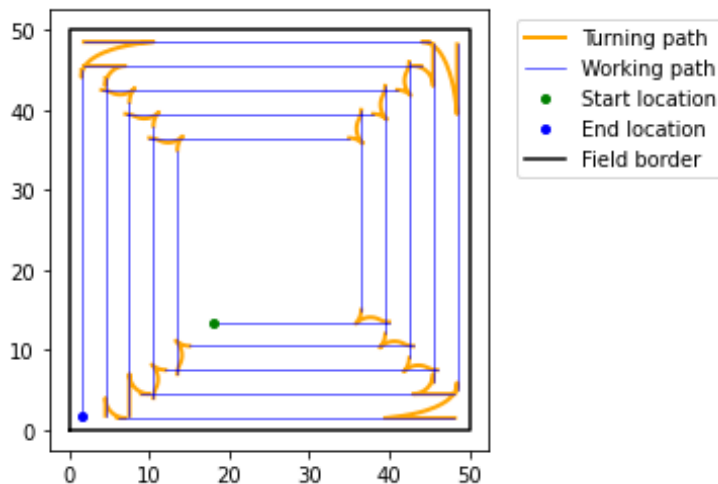


Figure 25: Headland CPP with a spiral pattern. This spiral pattern starts at the inner field border and is rotating counter-clockwise. The lower left corner is the start corner. At this corner, the CPAs are shifting from one swath to another and are therefore creating a spiral pattern.

2.5.1 Start and finish location at the start corner

For determining the start and finish location, it is important to maximize the coverage of the working area while avoiding the crossing of the field border. For a concave start corner, the start and finish location of the headland CPP are not limited by the field border. Therefore, these two locations are determined by Points A and B from the free space FT-CPA, where Point B is the start location, and Point A is the finish location.

For a convex start corner, there are two possible start locations and two possible finish locations. Both can be either at the pass next to the field border or the inner field border. The start location next to the field border is similar to Point B from the limited space FT-CPA_{cv}. The finish location on the pass next to the field border is similar to Point A from the limited space FT-CPA_{cv}.

The start or finish location next to the inner field border is calculated using Algorithm A-2 in the Appendix, with Table 9 as input. The finish location holds the values of Point A, and the start location holds the values of Point B.

Table 9: Values for calculating the start or finish location at the start corner next to the inner field border.

Angle α_{int}	lpA	lpB	w_{LA}	w_{LB}	F_1
0 to 0.5π	RLW	FLW	y_{FLW}	y_{FLW}	1
0.5π to π	RRW	FRW	y_{FLW}	y_{FLW}	-1
π to 1.5π	RLW	FLW	y_{FRW}	y_{FRW}	1
1.5π to 2π	RRW	FRW	y_{FRW}	y_{FRW}	-1

Depending on whether the headland CPP starts at the inner field border or the field border, the correct start and end location are selected. For each location, the intersection is relocated using section 2.4.1.5 and is reprojected using section 2.4.5.

2.5.2 Route generator

The route starts in the start corner at the start location calculated in section 2.5.1. Depending on the field operation direction (clockwise or counter-clockwise), each next corner is selected. From this corner, the right CPA at the current swath is added to the route. Each round the current swath shifts inwards or outwards, depending on the start border. Each time when the route generator is again at the start corner, always an FT-CPA is inserted. Only an FT-CPA is used at the start corner because it can connect two different swath numbers, whereas this is not possible for the C-CPA. This FT-CPA is calculated again because, at the start corner, the current swath number is changing. Therefore, the FT-CPA has a different location compared to a similar corner without a changing swath number. Furthermore, the feasibility of the free space FT-CPA is now determined by different numbers of swaths around the arriving and leaving pass. Therefore, the FT-CPA at the start corner is calculated to its current situation.

When the route generator is in its final swath, the finish point is added when the route generator is at the start corner. This together results in a final CPP on the headland, which goes from the start location to the finish location determined in section 2.5.1.

To create a headland CPP, the following items are required (Table 10):

Table 10: Required items for creating the headland CPP

Item number	Item	Explanation
1	Field border	Points need to be given in clockwise rotation
2	Headland width	Can be calculated using section 2.3
3	Number of swaths	Linked to headland width
4	Dimensions of RIC	Explained in section 2.3.1
5	Field limit for the robot and implement	Allowed exceedance of the field border
6	Work radius	Turning radius while still at work
7	Start corner	One of the points describing the field border
8	Field operation direction	Clockwise or counter-clockwise
9	Start border	Inner field border or field border

3 Application of the methodology to a variety of dimensions and settings

In this chapter, the methodologies explained in chapter 2 are applied to a variety of RIC dimensions and other settings. In section 3.1, each different turning manoeuvre for the CPAs is evaluated, where relevant variables are varied to analyse the behaviour of the turning manoeuvre. Furthermore, the route generator from section 2.5.2 is assessed in section 3.2, which also shows examples of a headland CPP.

For evaluating the methodologies of chapter 2, a RIC was used that is based on a robot with a cultivator attached to the rear. The dimensions were obtained on dimensions found in AgXeed (2022b) and using visual interpretation (Table 11). Figure 26 shows a visualisation of these dimensions. For the analysis, one or two dimensions from Table 11 were changed in value to observe the effect. All other dimensions were kept the same.

Table 11: Dimensions for a RIC, which are used for evaluating the methodology from chapter 2. These dimensions are visualised in Figure 26.

DIMENSION	VALUE [M]
w_{robot}	2.25
d_{crf}	1.8
d_{crr}	1.8
d_{cri}	3.0
w_{im}	3.0
off_{im}	0.0
l_{im}	2.0
w_{work}	3.0
off_{work}	0.0
d_{wa}	0.0
l_{work}	2.0
R	2.5

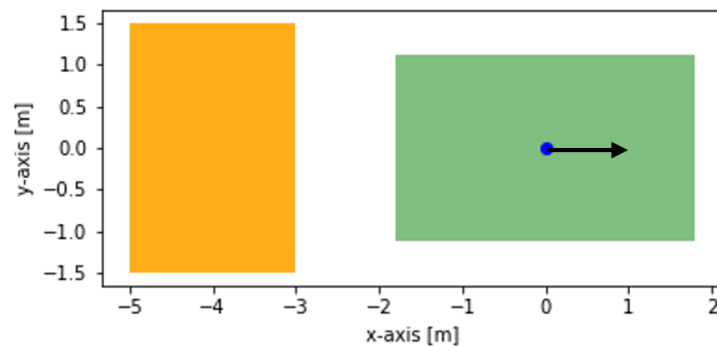


Figure 26: Visualisation of the dimensions from Table 11, which shows a top view of the RIC. The orange area is the implement and the working area, the green area is the robot, the blue dot is the center of rotation, and the arrow is the heading direction.

3.1 Assessment of individual turning manoeuvres for a Corner Planning Approach

Five different turning manoeuvres were considered in chapter 2. In this section, each of these turning manoeuvres is assessed by changing relevant variables.

3.1.1 Assessment of free space FishTail Corner Planning Approach

Two relevant variables influencing the travelled distance for a free space FT-CPA are the radius R and the length of the working area l_{work} . Each of these variables was assigned three different values for a corner angle ranging between 0 and π . The resulting travelled distances are shown in Figure 27:

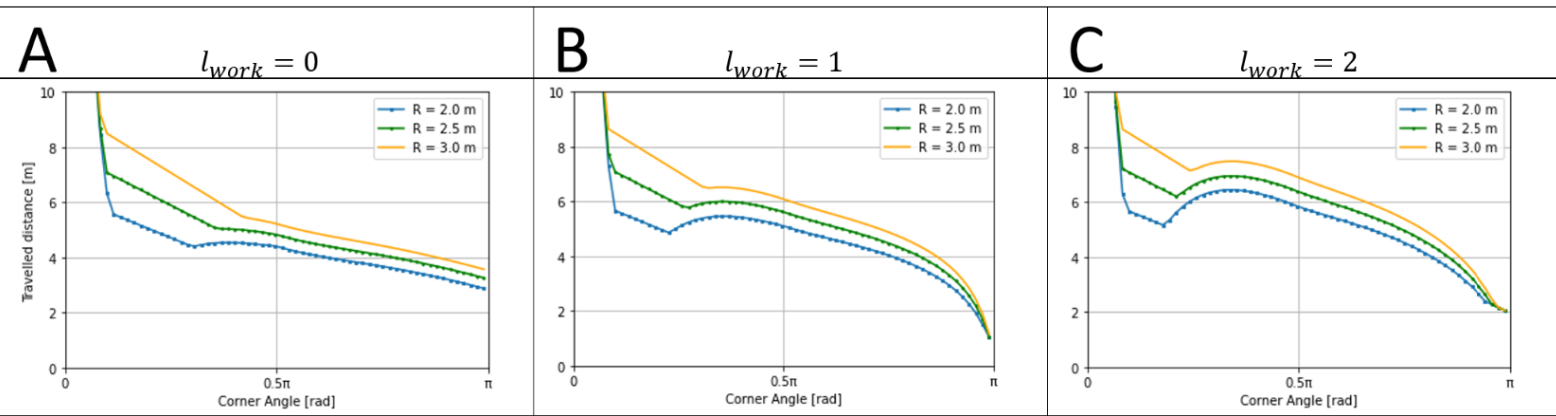


Figure 27: The travelled distance for a free space FT-CPA is changing when the values for l_{work} and R are varied and also depends on the corner angle. Each figure shows three different values for R (2.0, 2.5, and 3.0). (A), (B), and (C) show the travelled distance for a changing value from l_{work} with the values 0, 1, and 2 respectively.

Figure 27 shows that increasing both R and l_{work} leads to an longer distance required for the turning manoeuvre. With an increased R , the RIC needs to travel a larger distance to change the heading direction. With an increased l_{work} , the working area has a larger area. Because the soil is only properly covered when the full working area has crossed the soil, more overlap is required for the working area between Points A and B. Therefore, the travelled distance for the turning manoeuvre increases.

Another important factor for the free space FT-CPA is the required space for a turning manoeuvre because the RIC is not allowed to cross the field border. The required space was calculated using the algorithm described in section 2.4.1.6. In general, larger dimensions require more space. Furthermore, a relatively long RIC compared to the implement width requires more swaths for the turning manoeuvre. The effect of decreasing the length of the RIC is shown in Figure 28, where the value from d_{cri} is changed and plotted against a varying corner angle.

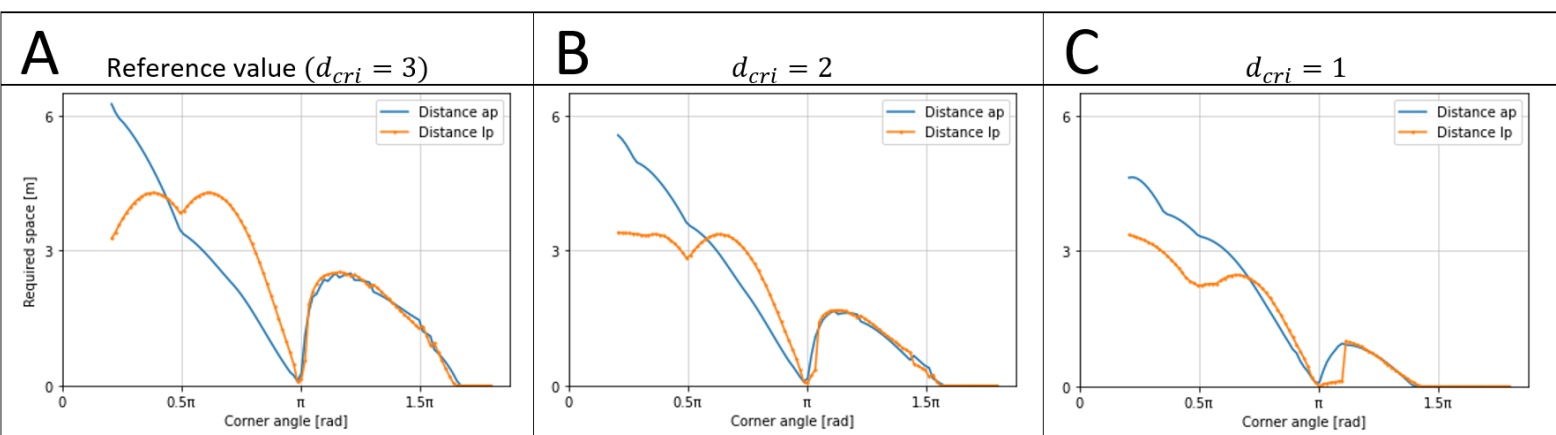


Figure 28: The required space of a free space FT-CPA for the arriving pass (ap) and leaving pass (lp) depends on the corner angle. (A) shows the required space with the reference values from Table 11, (B) and (C) show the required space where the value from d_{cri} is changed to 2 and 1 respectively. When the value for d_{cri} is decreasing, the RIC becomes more compact and therefore the free space FT-CPA requires less space for the turning manoeuvre.

Figure 28 shows that decreasing the distance between the center of rotation and the implement requires less space for a free space FT-CPA turning manoeuvre. This supports that a more compact RIC

requires less space. Furthermore, the required space strongly depends on the corner angle. For a corner angle between 0 and π in Figure 28 (A), the front side of the robot is determining the required space for the arriving pass, and the rear side of the implement is determining the required space for the leaving pass. For the corner angle between π and 2π , the rear side of the implement is determining the required space for both the arriving and leaving pass. For a corner angle between 0 and 0.5π in Figure 28 (C), the front side of implement is determining the required space for the leaving pass. Therefore, every change in a dimension of the RIC can lead to a different required space for the free space FT-CPA. In Appendix A, the required space is determined for different values of off_{work} and off_{im} , and w_{work} and w_{im} .

Some parts of Figure 28 show an irregular pattern (corner angle $> \pi$), which is caused by the discretization of the path for the turning manoeuvre.

3.1.2 Assessment of limited space FishTail Corner Planning Approach for convex corners

The most important variable for the limited space FT-CPA_{cv} is the field limit d_{fl} . In this study, the limited space FT-CPA_{cv} is determined by the allowed crossing of the field border parallel to the arriving pass. It assumes that the leaving pass is not crossed during a turning manoeuvre. However, this is not always true. This depends on the front side of the RIC and the angle of the corner. Therefore, the variable d_{crf} is changed to assess the quality of the turning manoeuvre. This was done by setting the value for d_{ifl} to 0.5 , and the value for d_{rfl} to 0.0 . With the RIC described in Table 11, the required distance at the arriving pass is determined by the implement, and the required distance at the leaving pass is determined by the robot. The results of changing the value from d_{crf} are shown in Figure 29.

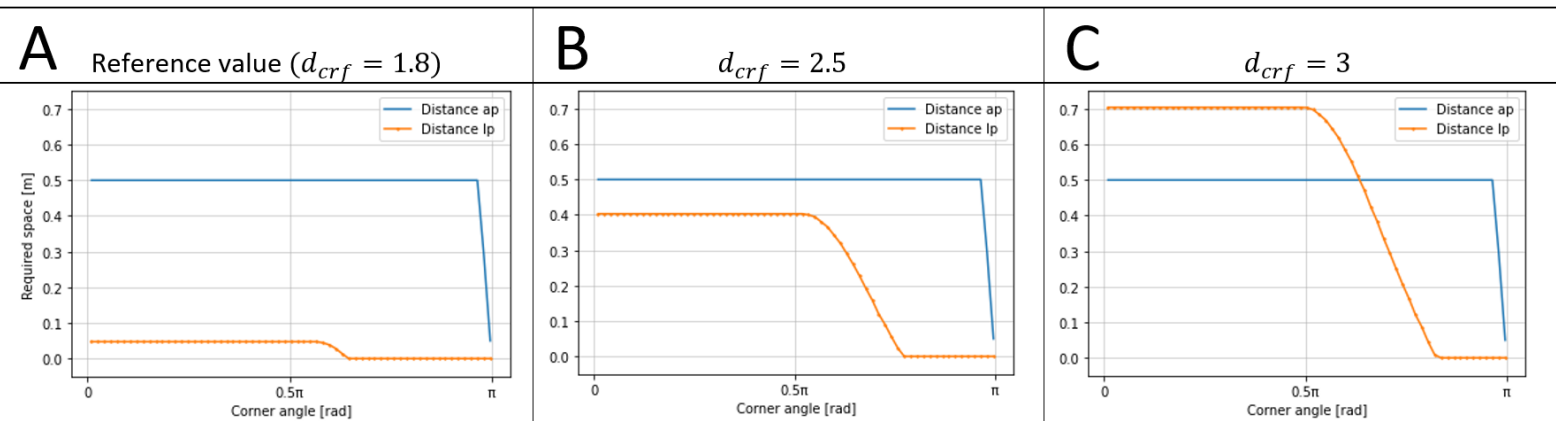


Figure 29: The required space for a limited space FT-CPA_{cv}. (A) shows the required space with the values from Table 11. (B) and (C) show the required space where the value from d_{crf} is 2.5 and 3 respectively. Increasing the value for d_{crf} shows that the required space for the leaving pass increases, but does not influence the required space for the arriving pass.

The results in Figure 29 show that the limited space FT-CPA_{cv} never crosses the set limit at the arriving pass. The implement never crosses the field limit of 0.5 m. However, the robot requires more space at the leaving pass when the value from d_{crf} increases. The limited space FT-CPA_{cv} assumes the robot does not cross the field limits at the leaving pass. However, Figure 29 shows that the leaving pass does require space for the turning manoeuvre, which depends on the dimensions of the RIC. Therefore, depending on the field limits and the dimensions of the RIC, the limited space FT-CPA_{cv} does not always have a feasible turning manoeuvre.

Furthermore, the variable d_{fl} has a significant influence on the travelled distance of the turning manoeuvre. Therefore, the value for d_{fl} was varied to assess the travelled distance with a varying corner angle. Moreover, the distance between the implement and the center of rotation (d_{cri}) also

has a significant influence on the travelled distance. The results for varying these two variables are shown in Figure 30.

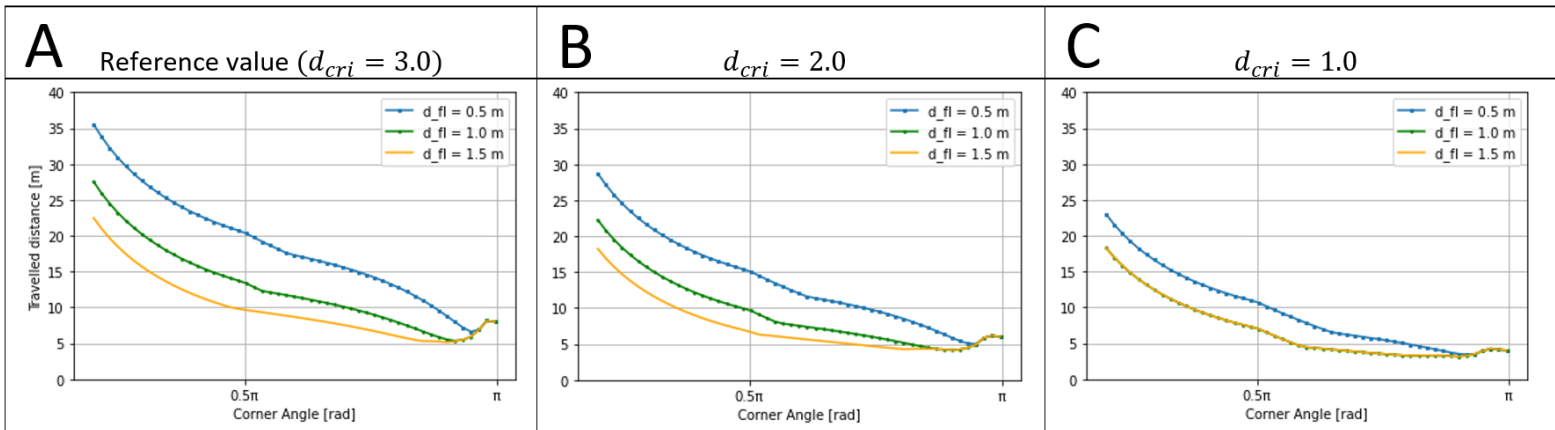


Figure 30: Increasing the field limit (d_{fl}) or decreasing the distance between the implement and the center of rotation (d_{cri}) leads to a decrease in the travelled distance for a limited space FT-CPA. (A) shows the travelled distance with the reference values from Table 11 for three different values of d_{fl} . (B) and (C) show the travelled distance where the value from d_{cri} is changed to 2.0 and 1.0 respectively.

Figure 30 shows that increasing the field limit leads to a shorter travelled distance for the turning manoeuvre. Furthermore, increasing the field limit at a small value (e.g. 0.5 m to 1.0 m) has a bigger impact on the decrease of the travelled distance than increasing the field limit at a greater value (e.g. 1.0 m to 1.5 m). The reason for this is that having a larger field limit, the RIC is relatively less restricted by the field border compared to a smaller field limit for the total travelled distance.

Decreasing the distance between the implement and the center of rotation (and therefore also bringing the rear of the implement closer to the center of rotation,) leads to a decrease in the travelled distance. Furthermore, the RIC is not limited by the field border when the implement is close enough to the center of rotation combined with a certain value of the field limit. This is shown in Figure 30 (C) ($d_{fl} = 1.0$ and $d_{fl} = 1.5$).

3.1.3 Assessment of limited space FishTail Corner Planning Approach for concave corners

The limited space FT-CPA_{cc} is created to never cross the field border at concave corners. Therefore, the crossing of the field border is not assessed for this type of turning manoeuvre. The only variable that significantly influences the travelled distance for the turning manoeuvre is the turning radius R . The results for varying the radius R are shown in Figure 31.

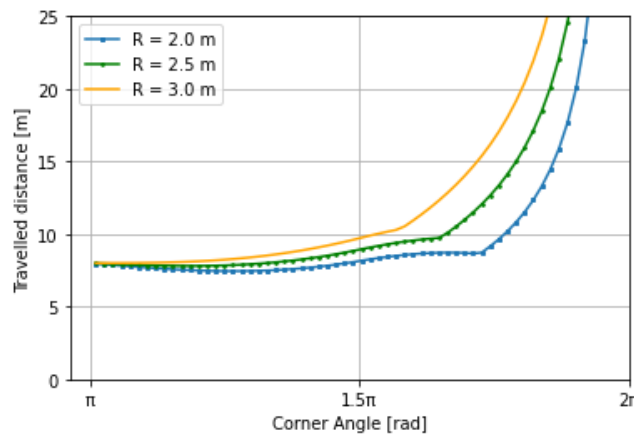


Figure 31: The influence of the turning radius R and the corner angle on the travelled distance for a limited space FT-CPA_{cc}.

Figure 31 shows two different trends; an almost horizontal trend for a corner angle between π and 1.5π , and an exponential trend between 1.5π and 2π . When the turning radius decreases, the point where the trend change is shifting to a larger corner angle. Therefore, a smaller turning radius requires less distance for the turning manoeuvre of a limited space FT-CPA_{cc}.

3.1.4 Assessment of Continuous Corner Planning Approach

The turning manoeuvre of the C-CPA assumes that the crossing of the field border with the implement is not an issue. However, depending on the radius R_{sw} , also the C-CPA requires additional space at the field border. Furthermore, also for the C-CPA, the distance between the implement and the center of rotation (d_{cri}) influences the required space. Therefore, the radius R_{sw} and the distance d_{cri} were varied to assess the required space for a C-CPA. A headland width of one swath was used for this assessment. These results are shown in Figure 32.

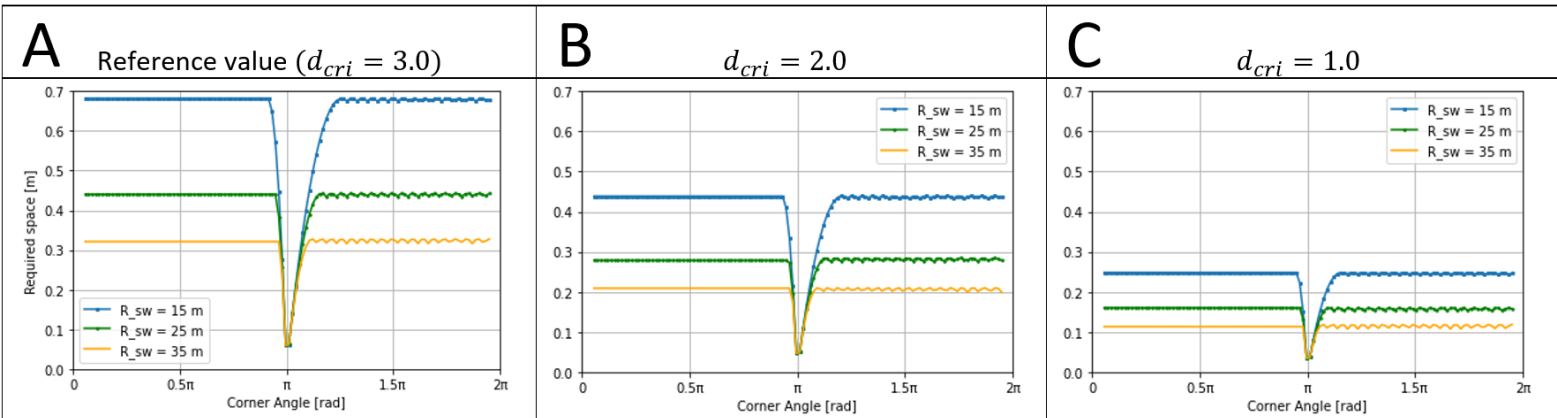


Figure 32: Increasing the radius R_{sw} and decreasing the distance d_{cri} leads to less required space for a C-CPA. (A) shows the required space with the reference values from Table 11 for three different values from R_{sw} . (B) and (C) show the required space where the value of d_{cri} is changed to respectively 2.0 and 1.0.

Figure 32 shows the effect of changing the radius R_{sw} on the required space depends on the distance d_{cri} . The reason for this is that an implement closer to the center of rotation swings less out when driving over a curved path.

For a convex corner, the R_{sw} for the swath closest to the field border depends on the total number of swaths. With a working width of 3 m, a minimum R_{sw} of 15 m, and a total of 5 swaths on the headland, the R_{sw} for the swath closest to the field border has a value of $15 + (5-1) * 3 = 27$ m. Therefore, the required space for a convex corner with a C-CPA also depends on the number of swaths. This is also the case for a concave corner because the first and third part of the turning manoeuvre are similar to a convex corner. The second part for a concave corner never requires additional space and is therefore not of interest for assessing the required space of a C-CPA at a concave corner.

In this study, the minimum R_{sw} was determined using the minimum effective working width. Therefore, the minimum R_{sw} is plotted against the minimum effective working width to show the relation between these two variables (Figure 33). Furthermore, the distance between the implement and the center of rotation (d_{cri}) also influences the minimum R_{sw} . This is also shown in Figure 33.

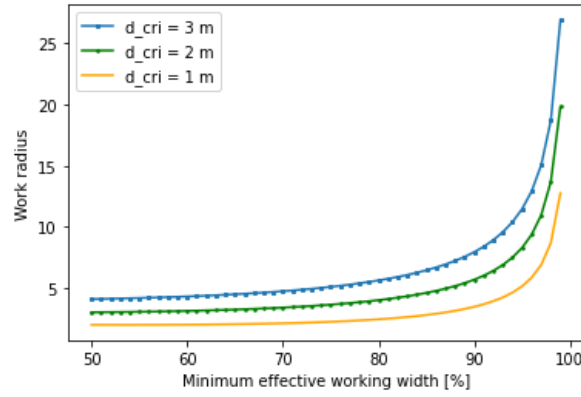


Figure 33: The minimum work radius R_{sw} depends in this study on the minimum effective working width. Furthermore, the distance d_{cri} also influences the working radius.

Figure 33 shows that especially a minimum effective working width between 90-100% influences the radius R_{sw} . Therefore, it is important to select a proper minimum effective working width. Moreover, when the implement gets closer to the center of rotation, the minimum effective working width becomes sensitive at a higher value compared to an implement further away from the center of rotation. This is because the change in minimum effective working width becomes less significant on the radius R_{sw} when the implement is closer to the center of rotation.

Because the turning radius from the swath next to the field border depends on the minimum radius for R_{sw} and the total number of swaths, the non-covered area changes when these two values change. Therefore, the non-covered area for the C-CPA was determined for a varying R_{sw} and a varying number of swaths. The results are shown in Figure 34.

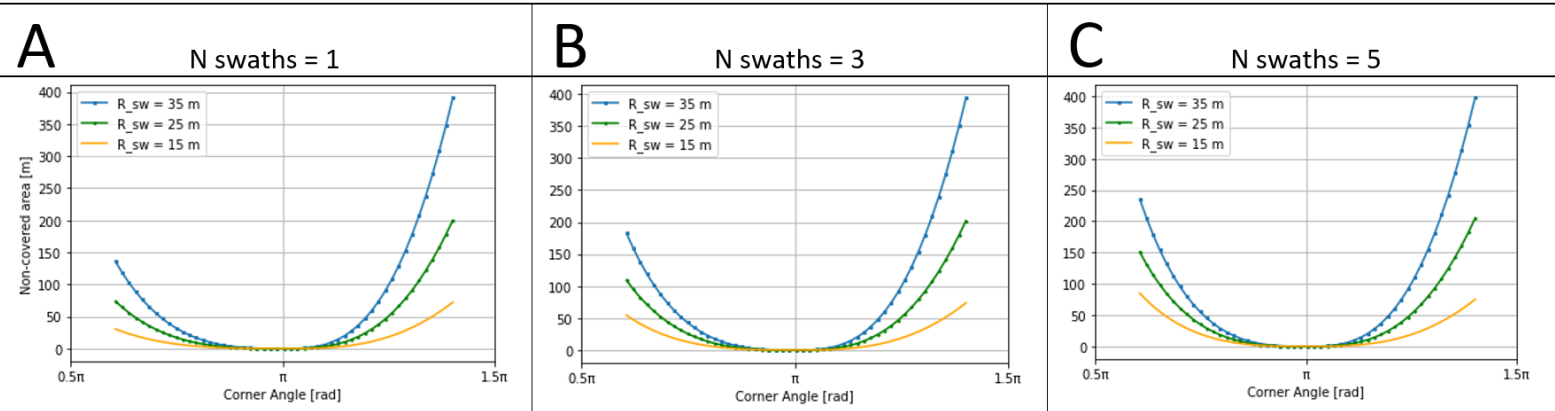


Figure 34: The minimum radius R_{sw} is varied for three different values (15, 25, 35). Furthermore, the number of swaths is changed in (A), (B), and (C) with 1, 3, and 5 respectively. Changing these values lead to a different value for the non-covered area of a C-CPA. Furthermore, the non-covered area also depends on the corner angle.

Figure 34 shows that the non-covered area for a convex corner is sensitive to the number of swaths, but a concave corner is not sensitive to the number of swaths. This is because the non-covered area for a convex corner is determined by the radius R_{sw} + the width of all the swaths, whereas the non-covered area for a concave corner is dominantly determined by the turning manoeuvre around C_2 , which uses the radius R_{sw} for the swath next to the field border. Therefore, the non-covered area for a concave corner is not sensitive to the number of swaths.

Furthermore, Figure 34 shows that the radius R_{sw} has a significant influence on the non-covered area. However, the corner angle has the strongest influence on the non-covered area.

3.1.5 Assessment of the objective function

The objective function determines which CPA is the best for a given corner. Therefore, the corner angle was varied for the assessment of the objective function. For this assessment, the headland width was set to 15 meters, the total number of swaths was 5, the value for $d_{rfl} = 0$, the value for $d_{ifl} = 0.5$, and the minimum effective working width was set to 97%. The results are shown in Figure 35.

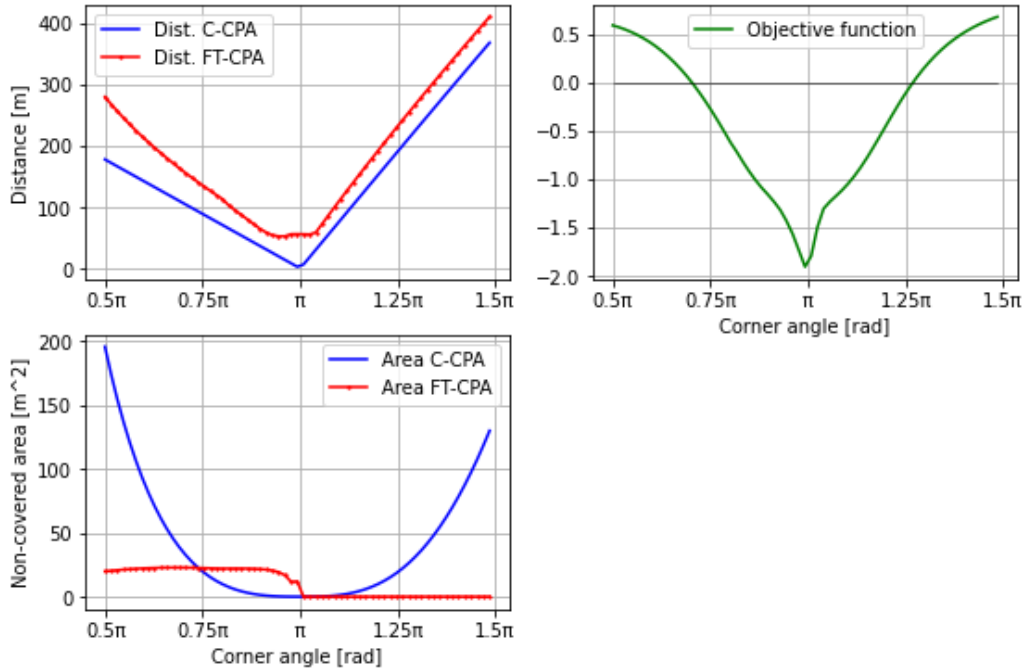


Figure 35: The objective function (top right) chooses either a C-CPA ($f < 0$) or an FT-CPA ($f > 0$). The outcome depends on the corner angle. For the calculation of the objective function, the travelled distance for each CPA is required (top left), and the non-covered area for each CPA is required (lower left).

The objective function from Figure 35 shows that the corner angles $\pm 0.7\pi$ and $\pm 1.25\pi$ are the tipping points for choosing a C-CPA or an FT-CPA. By changing the variables, the non-covered area and the travelled distance for each CPA changes. Therefore, the tipping points will also change. The most important variables to change were assessed in sections 3.1.1 to 3.1.4.

3.2 Assessment of the route generator for headland Coverage Path Planning

The route generator for a headland CPP uses the CPAs that are assessed in section 3.1. Therefore, the assessment of the route generator is focused on the aspects that are only involved with the route generator. These aspects are the start corner, the operation direction, and the start border. They are explained in more detail in section 3.2.1. Furthermore, the functionality of the route generator is explained in more detail in section 3.2.2.

3.2.1 Settings for the headland Coverage Path Planning

The aspects only involved for the route generator of a headland CPP are the start corner, the operation direction, and the start border. Changing the operation direction or the start border does not lead to significant changes in the route, because the type of CPA in each corner remains the same. Therefore, the travelled distance of the route is barely influenced by the operation direction and start border. These settings are only required to fit the specific field operation.

However, changing the start corner can lead to significant changes in the route, especially for a corner where a C-CPA would be optimal. This is because the start corner always uses the FT-CPA. Therefore, the travelled distance might increase significantly when selecting a different start corner. An example field was used to show the influence of selecting a different start corner on the travelled distance. This example field is shown in Figure 36.

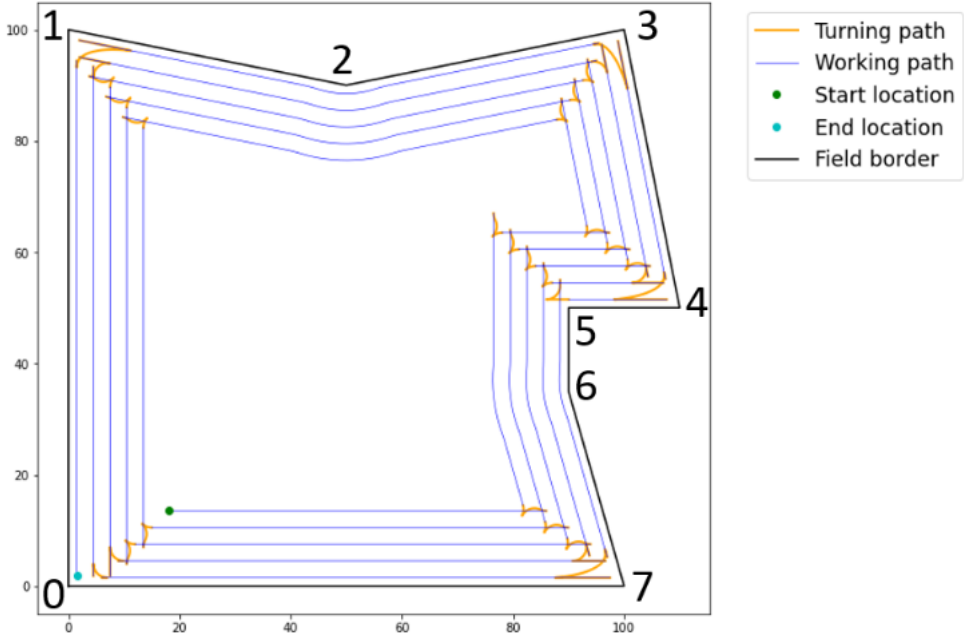


Figure 36: Example field with an area of 9425 m² to show the influence of selecting a start corner. The different start corners are indicated with a number. This figure starts at the start corner 0.

With the example field from Figure 36, the travelled distance was calculated for each different start corner, operation direction, and start border. The results are shown in Table 12.

Table 12: Selecting a different start corner might lead to an increased travelled distance. The percentages describe how much larger the travelled distance is from the lowest travelled distance (2095.7 m). Clockwise stands for the orientation direction, and field border means starting at the field border (TRUE) or starting at the inner field border (FALSE).

Clockwise	Field border	Start corner							
		0	1	2	3	4	5	6	7
TRUE	TRUE	0.92%	1.14%	2.69%	0.92%	1.14%	0.87%	2.58%	1.14%
TRUE	FALSE	0.00%	0.00%	2.69%	0.00%	0.00%	0.87%	2.58%	0.00%
FALSE	TRUE	0.92%	1.14%	2.69%	0.92%	1.14%	0.87%	2.58%	1.14%
FALSE	FALSE	0.00%	0.00%	2.69%	0.00%	0.00%	0.87%	2.58%	0.00%

Table 12 shows that a start corner at corner 2 or 6 leads to a significant increase in the travelled distance. Figure 36 shows that the best CPA for these corners is a C-CPA. However, a start corner always uses an FT-CPA, even when a C-CPA would be optimal. Therefore, it is important to select a proper field corner as a start corner to reduce the travelled distance.

When starting at the field border, the swath next to the field border at the start corner is directly limited by the field border without having an extra swath in between. However, this is not the case when starting at the inner field border. Therefore, starting at the field border requires one more limited space FT-CPA_{cv} that is directly next to the field border. Hence, a field operation starting at the field border requires in general a larger distance compared to starting at the inner field border (Table 12).

4 Discussion

In this study, a solution is proposed for determining the headland width and creating a headland CPP by taking the dimensions of the RIC into account. It was found that the dimensions of the RIC play a major role in feasible turning manoeuvres for a headland CPP, where the feasibility of a turning manoeuvre is constrained by crossing the field border with the RIC. In section 4.1, the important dimensions of the RIC are discussed in detail. Section 4.2 describes the design criteria for determining the headland width along with the limitations of this study in that respect. Section 4.3 describes the design criteria for turning algorithms for a headland CPP, and discusses the turning algorithms created in this study. Section 4.4 discusses the most important aspects of a headland CPP and evaluates the created headland CPP.

4.1 Important dimensions of a RIC for headland Coverage Path Planning

For headland CPP, it is important to consider the physical dimensions of the RIC for determining the required space for a turning manoeuvre. Furthermore, it is also important to take the functioning of the implement into account to allow a proper application of the field operation.

Compared to other studies where only the implement width of the RIC is considered (e.g., Jin and Tang (2010) and Nilsson and Zhou (2020)), this study proposes a representation of a RIC that is divided into three different areas; (1) the robot, (2) the implement, and (3) the working area, where each area has a rectangular shape (section 2.3.1). The dimensions of the robot and implement are used for determining the required space, and the working area is used for the proper functioning of the implement. Because the working area is not defined by a single width but by a two dimensional space, the main functioning of the implement also has a length that is required for a proper application of the field operation (e.g., a cultivator). Therefore, the coverage of the headland is determined by a pass of the full length from the working area (Figure 23). Hence, when only the front or rear side of the working area has covered an area, it is not seen as proper coverage of the headland.

A limitation of the RIC representation in this study is that the three different areas always have a rectangular shape. This applies to most common RICs, but some machinery has a different shape, e.g. a plow. Furthermore, the working area does also not always have a rectangular shape, e.g. for a fertilizer (disc) spreader. Therefore, the representation does not fit all RICs. It is currently unknown if the rectangular representation is good enough for more advanced shapes to create a proper headland CPP.

4.2 Design criteria for headland width

The most important design criterium for the headland width is to make sure that the field border is never crossed during a turning manoeuvre when covering the inner field. If this is not guaranteed, the headland width might be too small and therefore lead to infeasible solutions. Furthermore, the headland width should be large enough to allow optimal turning manoeuvres between swaths of the inner field, which has to be fully covered too. Moreover, all the RICs used over a growing season (e.g., a sprayer) must be able to manoeuvre and operate on the headlands.

The method proposed in this study for determining the headland width only uses a Dubins curve turning manoeuvre. However, there also exist other turning manoeuvres, like Reeds Shepp, which sometimes require a smaller distance for the turning manoeuvre. Therefore, for future work, it would be better to also include other turning manoeuvres. This also requires objective functions to select the optimal turning manoeuvre. Since the Fields2Cover library is also addressing soil compaction (de Bruin, 2022; Mier, 2022), it would be good to include it as an objective function.

4.3 Design criteria for headland Coverage Path Planning turning algorithms

The most important design criterium for headland CPP turning algorithms is similar to the headland width, namely no crossing or controlled crossing of the field border. With controlled crossing, a predefined distance is allowed for crossing the field border with the robot and/or implement, e.g. a hanging implement over a ditch (section 2.4.1.4). Furthermore, the headland coverage must be maximized for a higher quality of the field operation. This headland coverage is determined by the start and end location of the turning manoeuvre.

Another design criterium is to select the required objective functions for the field operation to optimise the headland CPP (Chakraborty et al., 2022). There exist numerous objective functions for the optimisation, e.g. fuel consumption, non-covered area, and travelled distance (Chakraborty et al., 2022). In this study, the optimisation was based on travelled distance and non-covered area (section 2.4.4).

Proposed solutions

Since the headland CPP is understudied, only studies were found that took the width of the implement into account to avoid crossing the field border during a turning manoeuvre. In this study, a solution is proposed that takes all the dimensions of the RIC into account to avoid crossing the field border when creating a headland CPP (section 2.4.1.4). It uses a fishtail pattern (FT-CPA) as a basis (section 2.4.1).

Following Nilsson and Zhou (2020) recommendation, the current study used a turning algorithm that allows reverse driving (section 2.4.1.3 - *free space FT-CPA*). However, the space required for this turning algorithm is not always available, leading to the crossing of the field border (section 3.1.1, Figure 28). Therefore, another turning algorithm was created that allows controlled crossing of the field border (sections 2.4.1.4 - *limited space FT-CPA_{cv}* and 2.4.1.5 - *limited space FT-CPA_{cc}*). The start and end locations of these turning algorithms are based on either full coverage of the headland or no field border crossing (section 2.4.1.2).

Yet another proposed turning algorithm (C-CPA) focused on minimizing the travelled distance (section 2.4.2). Instead of making a turning manoeuvre like the FT-CPA, this turning algorithm allows a continuation of the field operation, at the cost of a non-covered area. Therefore, this turning algorithm is especially suited for turning manoeuvres where the heading direction barely changes, resulting in a small non-covered area (section 3.1.4, Figure 34).

Implications

Although the limited space FT-CPA was created to avoid uncontrolled crossing of the field border, the RIC might cross the field border beyond an acceptable crossed distance (section 3.1.2, Figure 29). This is because the crossing of the field border is only controlled for the field border parallel to the arriving pass, and not for the leaving pass. Therefore, the crossing of the field border parallel to the leaving pass is uncontrolled. The feasibility of the crossing of this field border depends on the dimensions of the RIC and the allowed distance to cross the field border (section 3.1.2, Figure 29).

Furthermore, the C-CPA assumes that crossing the field border is no issue and therefore it does not take it into account. In reality, the C-CPA always crosses the field border, where the severity depends on the dimensions of the RIC and the work radius (section 3.1.4, Figure 32). If these crossings of the field border are larger than the allowed crossing, the turning manoeuvre is infeasible. To avoid an infeasible solution for a C-CPA, the work radius could be increased (section 3.1.4, Figure 32). The current algorithm is not able to calculate this minimum work radius to allow a feasible turning manoeuvre.

The developed optimisation of the turning manoeuvre does not consider the area damaged by the wheels/tracks of the RIC. This damaged area is the area the RIC requires of the already covered area when making a turning manoeuvre. However, this damaged area would be useful to use as an objective function to minimize this area and therefore increase the quality of the crop and turning manoeuvre.

4.4 Application of objective function and headland Coverage Path Planning

The outcome of the objective function and headland CPP depends on all the dimensions of the RIC(s) (section 3.1), the different settings required for creating the CPAs and the headland CPP (section 2.5.2), and the radius R or R_{sw} (Figure 27, Figure 31, and Figure 34). Furthermore, the outcome of the objective function depends severely on the field corner angle (section 3.1.5, Figure 35). Therefore, changing the dimensions and settings will lead to different outcomes. This change depends on the value of the corner angle and the relative change of dimensions and settings. When the corner angle is close to the tipping point of the objective function, it is more likely that the outcome of the objective function selects a different CPA when some values of the dimensions or settings are changed (Figure 35).

When making a headland CPP, it must fit the needs of the specific field operation. However, field operations differ widely and therefore the headland CPP requires flexibility. With the flexibility of the headland CPP in this study, the field operation can start at any field corner, it can have an inward or outward operation direction, it can be planned in a clockwise or counter-clockwise direction, and the number of swaths can be less than the headland width (section 3.2.2). However, the current headland CPP can only create a route for a robot with a rear-mounted implement, where the seeding pattern does not depend on the harvesting pattern. Furthermore, not every field corner is suited as a start corner, because selecting a different start corner can affect the travelled distance of the headland CPP (section 3.2.1, Table 12).

A limitation of the headland CPP in this study is that it is only created with an FT-CPA as the basis. However, this does not fit every field operation. Some crops, like row crops (e.g. potatoes or sugar beets), cannot be properly harvested when using the FT-CPA, because these harvesters normally require a relatively large space for turning manoeuvres, and would therefore cause crop damage and degraded crop quality, which could result in a lower profit (NAK, 2016). Therefore, different CPAs are required that fit these specific field operations. Furthermore, the seeding pattern of the row crops usually depends on the harvesting pattern. Therefore, the seeding and harvesting pattern need to be planned simultaneously, which requires an even more advanced CPA algorithm. For creating the algorithm of these two patterns, the orientation of all crop rows must be equal, each field operation must be feasible (controlled field border crossing), and each field operation must be optimised on relevant objective functions, like crop damage, non-covered area, and travelled distance.

The current FT-CPA is focused on ending the CPA with the field operation to allow a greater coverage of the corner with a seeder. However, for harvesting (e.g. combine harvester), it is better to harvest as much as possible before making the turn, to avoid crop damage. Therefore, the current headland CPP is not directly able to create a proper route for a harvester. This requires different start and end locations of the turning manoeuvre, which is not yet implemented in the software.

To avoid unfeasible solutions with the current headland CPP, the field limit could be increased. If the field limit cannot be increased anymore and the headland CPP is still not feasible, more space at the field border could be left open to allow more space for the turning manoeuvre. However, this is not an ideal solution as it would decrease the covered area. Therefore, turning algorithms are required that can deal better with the crossing of the field border. For the limited space FT-CPA_{cv}, a turning algorithm could be created that also has reverse turning. This creates more space for the turning

manoeuvre, which allows a faster turning manoeuvre, and could therefore lead to a smaller travelled distance. For the C-CPA, the work radius could be increased to allow a feasible turn (section 3.1.4, Figure 32). With a larger work radius, the implement will swing less out and therefore requires less space.

5 Conclusion and recommendations

- For the creation of a headland CPP, it is important to use the previously often ignored physical dimensions of the RIC, to avoid or to have control over the crossing of a field border. Furthermore, for proper field coverage by the implement, it is better to have a two-dimensional working area instead of a one-dimensional width because an implement requires a length for its field operation.
- Determination of the headland width should take into account the objective to fully cover the inner field. There must be enough space for the optimal turning approaches, and the width must be feasible for every RIC required for a growing season.
- The most important design criteria for turns in field corners is to have a controlled crossing of the field border, maximized coverage, and high crop quality.
- The headland CPP developed in this study can create a route for a seeding or tillage operation with a rear-mounted implement, which has feasible solutions with the right combination of dimensions and settings.

The most surprising result is that changing a dimension or setting does not always lead to a change in the outcome of the headland CPP. This is because the effect of the change in dimension or setting on the headland CPP strongly depends on the corner angle. Therefore, the effect of changing a dimension or setting depends on the field geometry and can therefore vary between different field geometries.

For future work, it should be investigated if more advanced shapes are required for the representation of the RIC that better matches the true dimensions, or if the current representation is also suited for these specific RICs. Furthermore, the headland width should be determined with turning manoeuvres that also allow reverse driving. Currently, this is done for a forward driving-only turning manoeuvre. However, the Fields2Cover library also has reverse-driving turning algorithms. Therefore, the turning manoeuvre on the headland for covering the inner field should be optimised for the different turning algorithms to determine the required headland width.

Moreover, a more advanced limited space FT-CPA_{cv} is required that allows reverse turning and can therefore create more space for the turning manoeuvre. This turning manoeuvre must be able to have controlled crossing for every part of the field border. Also, optimisation is required to find the minimum work radius for a C-CPA that allows controlled crossing of the field border. Furthermore, more CPAs are required that better fit to field operations for specific crops, like row crops, because for some crops the seeding pattern depends on the harvesting pattern, which requires a more advanced CPA algorithm. Moreover, crop damage should also be part of the optimisation because it can lead to degraded crop quality and therefore a lower profit.

References

- AGGPS. (2022). *3A GPS: Affordable Accurate Agriculture GPS*. Retrieved 7 September 2022 from <https://aggps.ca/>
- Agrotheek. (2023). *Driftreducties en teeltvrije zone*. Retrieved 16 January 2023 from <https://www.agrotheek.nl/Actueel/driftreducties-en-teeltvrije-zone>
- AgXeed. (2022a). *AgXeed webpage*. Retrieved 8 September 2022 from <https://agxeed.com/>
- AgXeed. (2022b). *AGXEED AgBot 5.115T2*. Retrieved 26 September 2022 from <https://agxeed.com/agbot-5-115t2/>
- Augère-Granier, M.-L. (2021). Migrant seasonal workers in the European agricultural sector. *European Parliamentary Research Service, PE 689.347*. [https://www.europarl.europa.eu/RegData/etudes/BRIE/2021/689347/EPRS_BRI\(2021\)689347_EN.pdf](https://www.europarl.europa.eu/RegData/etudes/BRIE/2021/689347/EPRS_BRI(2021)689347_EN.pdf)
- Case IH. (2022). *Autonomous Farming*. Retrieved 8 September 2022 from <https://www.caseih.com/anz/en-au/innovations/autonomous-farming>
- Chakraborty, S. E., Devaraj Govindarajan, P. L., Elnaggar, M. F., Alrashed, M. M., & Kamel, S. (2022). A Comprehensive Review of Path Planning for Agricultural Ground Robots. *Sustainability, 14*(15). <https://doi.org/10.3390/su14159156>
- Christiaensen, L., Rutledge, Z., & Taylor, J. E. (2020). *The Future of Work in Agriculture: Some Reflections*. https://www.researchgate.net/publication/340172344_The_Future_of_Work_in_Agriculture_Some_Reflections
- de Bruin, S. (2011). *Map-based CTF met GAOS*. Retrieved 19 October 2022 from <https://edepot.wur.nl/307475>
- de Bruin, S. (2022). *Fields2cover: Robust and efficient coverage paths for autonomous agricultural vehicles*. Retrieved 6 September 2022 from <https://www.wur.nl/en/project/Fields2cover-Robust-and-efficient-coverage-paths-for-autonomous-agricultural-vehicles.htm>
- Department of Mathematics. (2022). *Rotation of Axes*. Retrieved 31 October 2022 from <https://math.sci.cuny.cuny.edu/document/Rotation+of+Axes#:~:text=Coordinate%20Rotation%20Formulas&text=x%20%3D%20CB%86xcos%20CE%B8%20E2%88%92%20CB%86y%20sin%CE%B8,%3D%20CB%86xsin%CE%B8%20%2B%20CB%86y%20cos%20CE%B8>
- Diserens, E., Battiato, A., & Sartori, L. (2014). Soil Compaction, Soil Shearing and Fuel Consumption: TASC V3.0 – A Practical Tool for Decision-Making in Farming. Proceedings International Conference of Agricultural Engineering, Zürich, Switzerland.
- DrawIO. (2023). <https://app.diagrams.net/>
- Dubins, L. E. (1957). On Curves of Minimal Length with a Constraint on Average Curvature, and with Prescribed Initial and Terminal Positions and Tangents. *American Journal of Mathematics, 79*(3), 497-516. <https://doi.org/10.2307/2372560>
- Fendt. (2022). *For those who prefer precision – Guidance from Fendt*. Retrieved 7 September 2022 from <https://www.fendt.com/us/smart-farming/guidance#varioguide-fendt-contour-assistant>
- Galceran, E., & Carreras, M. (2013). A survey on coverage path planning for robotics. *Robotics and Autonomous Systems, 61*(12), 1258-1276. <https://doi.org/10.1016/j.robot.2013.09.004>
- Godwin, R., Misiewicz, P., White, D., Dickin, E., Grift, T., Pope, E., Millington, A., Shaheb, R. M., & Dolowy, M. (2019). The effect of alternative traffic systems and tillage on soil condition, crop growth and production economics. 7th International Conference on Trends in Agricultural Engineering 2019, TAE 2019, Prague.
- Google Maps. (2023). Retrieved 16 March 2023 from <https://www.google.com/maps/@53.3344108,6.8594528,254m/data=!3m1!1e3>
- GRIMME. (2022). *HARVESTING TECHNOLOGY - 2-ROW | SE 260*. Retrieved 10 October 2022 from <https://www.grimme.com/uk/producttypes/erntetechnik-kartoffel/se-260>

- Heraud, J. A., & Lange, A. F. (2009). Agricultural Automatic Vehicle Guidance from Horses to GPS: How We Got Here, and Where We Are Going. *ASABE Distinguished Lecture*, 33, 1-67. <https://citeseerx.ist.psu.edu/viewdoc/download?doi=10.1.1.214.3533&rep=rep1&type=pdf>
- Horsmans. (2023). *SE 260 OOGSTTECHNIEK 2-RIJIG*. Retrieved 16 January 2023 from <https://www.horsmans.nl/nl/landbouwmechanisatie/se-260-erntetechnik-2-reihig>
- Jin, J., & Tang, L. (2010). Optimal Coverage Path Planning for Arable Farming on 2D Surfaces. *Transactions of the ASABE*, 53(1), 283-295. <https://doi.org/10.13031/2013.29488>
- John Deere. (2022). *John Deere Reveals Fully Autonomous Tractor at CES 2022*. Retrieved 8 September 2022 from <https://www.deere.com/en/news/all-news/autonomous-tractor-reveal/>
- KUHN. (2023). *Fertiliser spreader ACCURA 1600*. Retrieved 30 January 2023 from <https://www.kuhn.com/en/crop/fertiliser-spreaders/mounted-spreaders/mounted-twin-disc-spreaders/accura-1600>
- Mathway. (2022). *Calculus*. Retrieved 27 October 2022 from <https://www.mathway.com/Calculus>
- McPhee, J. E., Aird, P. L., Hardie, M. A., & Corkrey, S. R. (2015). The effect of controlled traffic on soil physical properties and tillage requirements for vegetable production. *Soil and Tillage Research*, 149, 33-45. <https://doi.org/10.1016/j.still.2014.12.018>
- Mier, G. (2022). *Fields2Cover*. Retrieved 6 September 2022 from <https://github.com/Fields2Cover/Fields2Cover>
- Mier, G., Valente, J., & Bruin, S. d. (2023). Fields2Cover: An open-source coverage path planning library for unmanned agricultural vehicles. *IEEE Robotics and Automation Letters*, 8(4), 2166 - 2172. <https://doi.org/10.1109/LRA.2023.3248439>
- NAK. (2016). *De keuring van pootaardappelen*. Retrieved 19 September 2022 from <https://www.nak.nl/wp-content/uploads/archief/2012/Zakelijke%20informatie/Publicaties/Brochures/De%20keuring%20van%20pootaardappelen%202016.pdf>
- Nawaz, M. F., Bourrié, G., & Trolard, F. (2013). Soil compaction impact and modelling. A review. *Agronomy for Sustainable Development*, 33(2), 291-309. <https://doi.org/10.1007/s13593-011-0071-8>
- Nilsson, R. S., & Zhou, K. (2020). Method and bench-marking framework for coverage path planning in arable farming. *Biosystems Engineering*, 198, 248-265. <https://doi.org/https://doi.org/10.1016/j.biosystemseng.2020.08.007>
- Parvin, N., Coucheney, E., Gren, I.-M., Andersson, H., Elofsson, K., Jarvis, N., & Keller, T. (2022). On the relationships between the size of agricultural machinery, soil quality and net revenues for farmers and society. *Soil Security*, 6, 100044. <https://doi.org/10.1016/j.soisec.2022.100044>
- Reeds, J. A., & Shepp, L. A. (1990). Optimal Paths for a Car that goes both Forwards and Backwards. *Pacific Journal of Mathematics*, 145(2), 367-393. <https://doi.org/10.2140/pjm.1990.145.367>
- Scheuer, A., & Fraichard, T. (1997). Continuous-curvature path planning for car-like vehicles. *International conference on intelligent robots and systems*, 2, 1-7. <https://doi.org/10.1109/IROS.1997.655130>
- Schouten, E. (2022). *Dubins*. Retrieved 12 October 2022 from <https://github.com/ESchouten/Dubins>
- Scott, H., DeAngulo, J., Daniels, M., & Wood, L. (1989). Flood duration effects on soybean growth and yield. *Agronomy Journal*, 81(4), 631-636. <https://doi.org.ezproxy.library.wur.nl/10.2134/agronj1989.00021962008100040016x>
- Shapely. (2022). *Shapely 2.0.0*. In (Version 2.0.0) <https://pypi.org/project/Shapely/>
- Sloans. (2018). *New Auto Trac Prices*. Retrieved 7 September 2022 from <https://standardsite-images-prod.s3.amazonaws.com/sloans.com/80daef28-0145-4a70-86fb-74eae4b95c37.pdf>
- Steinbusch, M. (2020). Teelt- en spuitvrije zones. *GRONDIG*, 3, 54-55. <https://edepot.wur.nl/520012>
- SymPy. (2021). *SymPy*. In <https://www.sympy.org/en/index.html>
- van Velde, P. (1998). Rijenafstanden en normalisatie, waar naar toe *Landbouwmechanisatie*, 2. <https://edepot.wur.nl/506727>
- Waterschap Zuiderzeeland. (2019). SPUITBOOM BOVEN SLOOT EN GEBRUIK KANTDOP. *Agrariërs*, 1, 6. https://www.zuiderzeeland.nl/flysystem/media/agrarische_nieuwsbrief_voorjaar_2019.pdf

Zhai, Z., Martínez, J. F., Beltran, V., & Martínez, N. L. (2020). Decision support systems for agriculture 4.0: Survey and challenges. *Computers and Electronics in Agriculture*, 170, 105256. <https://doi.org/10.1016/j.compag.2020.105256>

Appendix | Algorithms

Algorithm A-1 | Calculating the offset from the center of the curve for an LRL configuration

$$\begin{aligned}
 d_{offAB,y} &= d_A - d_B \\
 d_{AB,x} &= w_{work} - 2 * |off_{work}| \\
 d_{ABif,y} &= \frac{d_{AB,x}}{\tan(\alpha_{int})} \\
 d_{AB,y} &= d_{ABif,y} + d_{offAB,y} \\
 d_{C_{13},x} &= d_{AB,x} + 2 * R \\
 d_{C_{13}} &= \sqrt{d_{AB,y}^2 + d_{C_{13},x}^2} \\
 d_{C_{12}} &= 2 * R \\
 \alpha_{C_{13},x} &= \tan^{-1}\left(\frac{d_{AB,y}}{d_{C_{13},x}}\right) \\
 \alpha_{C_{12},x} &= \cos^{-1}\left(\frac{\frac{1}{2} * d_{C_{13}}}{d_{C_{12}}}\right) - \alpha_{C_{13},x}
 \end{aligned}$$

Point A = (R, 0)

Point B = (R + d_{AB,x}, -d_{AB,y})

Point B_{if} = (R + d_{AB,x}, -d_{ABif,y})

Point C₂ = (d_{C₁₂} * cos(α_{C₁₂,x}), d_{C₁₂} * sin(α_{C₁₂,x}))

Algorithm A-2 | Calculate Points A and B for corner turning manoeuvres

$$\begin{aligned}
 x_A &= -x_{lpA} + \frac{y_{lpA}}{\tan(\alpha_{int})} - \frac{w_{LA}}{\sin(\alpha_{int})} \\
 y_A &= 0 \\
 \alpha_{lpB} &= \tan^{-1}\left(\frac{x_{lpB}}{y_{lpB}}\right) \\
 \alpha_{lpB,x} &= \alpha_{int} + F_1 * |\alpha_{lpB}| - F_1 * \frac{1}{2} * \pi \\
 d_{lpB} &= \sqrt{x_{lpB}^2 + y_{lpB}^2} \\
 y_B &= \sin(\alpha_{lpB,x}) * d_{lpB} + w_{LB} \\
 x_B &= \frac{y_B}{\tan(\alpha_{int})}
 \end{aligned}$$

Algorithm A-3 | Calculate Points C₁, C₂, and C₃ for the free space FT-CPA

$$x_{C_1} = x_A$$

$$y_{C_1} = F_2 * R$$

$$d_{C_3B,x} = R * \sin(\alpha_{int})$$

$$d_{C_3B,y} = R * \cos(\alpha_{int})$$

$$x_{C_3} = x_B - d_{C_3B,x} * F_2$$

$$y_{C_3} = y_B + d_{C_3B,y} * F_2$$

IF $x_{C_1} = x_{C_3}$ THEN:

$$y_{C_2} = 0.5 * (y_{C_1} + y_{C_3})$$

$$x_{C_2} = x_{C_1} - F_1 * \sqrt{(r_{C_2} + R)^2 - (y_{C_1} - y_{C_2})^2}$$

ELSE IF $y_{C_1} = y_{C_3}$ THEN:

$$x_{C_2} = 0.5 * (x_{C_1} + x_{C_3})$$

$$y_{C_2} = y_{C_1} - F_2 * \sqrt{(r_{C_2} + R)^2 - (x_{C_1} - x_{C_2})^2}$$

ELSE:

equation for the line on which C₂ is located

$$a_1 = -\frac{x_{C_3} - x_{C_1}}{y_{C_3} - y_{C_1}}$$

$$b_1 = 0.5 * \left(y_{C_1} + y_{C_3} + \frac{(x_{C_3} - x_{C_1})(x_{C_3} + x_{C_1})}{y_{C_3} - y_{C_1}} \right)$$

$$y_{C_2} = x_{C_2} * a_1 + b_1$$

Determine the value from x_{C₂}

Determined using the following equation:

$$d_{C_{12}} = R + r_{C_2} = \sqrt{(x_{C_1} - x_{C_2})^2 + (y_{C_1} - y_{C_2})^2}$$

$$a = 1 + a_1^2$$

$$b = -2 * x_{C_1} - 2 * a_1 * y_{C_1} + 2 * a_1 * b_1$$

$$c = x_{C_1}^2 + y_{C_1}^2 + b_1^2 - 2 * b_1 * y_{C_1} - R^2 - r_{C_2}^2 - 2 * R * r_{C_2}$$

IF ($y_{C_1} > 0$ AND $y_{C_1} > y_{C_3}$) OR ($y_{C_1} < 0$ AND $y_{C_1} < y_{C_3}$) THEN:

$$x_{C_2} = \frac{-b + \sqrt{b^2 - 4ac}}{2a}$$

ELSE:

$$x_{C_2} = \frac{-b - \sqrt{b^2 - 4ac}}{2a}$$

Needed angles for calculating the path

$$\alpha_{x,C_{12}} = \tan^{-1} \left(\frac{y_{C_1} - y_{C_2}}{x_{C_2} - x_{C_1}} \right) + \frac{1}{2} * \pi$$

Remark: \tan^{-1} is the python function `math.atan2`

$$\alpha_{x,C_{23}} = \tan^{-1} \left(\frac{y_{C_3} - y_{C_2}}{x_{C_2} - x_{C_3}} \right) - \frac{1}{2} * \pi$$

$$\alpha_{C_3B,y} = \tan^{-1} \left(\frac{y_B - y_{C_3}}{x_B - x_{C_3}} \right)$$

$$\alpha_{C_{21},y} = \tan^{-1} \left(\frac{x_{C_2} - x_{C_1}}{y_{C_2} - y_{C_1}} \right)$$

Algorithm A-4 | Limiting point on RIC for turning in part 2

$$p_r = |RRR| = |RLR|$$

IF $0 < \alpha_{int} < \pi$ THEN:

$$p_{im} = |RRI|$$

ELSE:

$$p_{im} = |RLI|$$

Definitions for the limiting points on the robot and implement, including the distance from the limiting points to the center of the curve.

$$d_{r.cc} = \sqrt{x_{p_r}^2 + (y_{p_r} + R)^2}$$

$$d_{im.cc} = \sqrt{x_{p_{im}}^2 + (y_{p_{im}} + R)^2}$$

IF ($x_{RRI} > 0$) OR ($d_{im.cc} < d_{r.cc}$) THEN:

$$\begin{aligned} d_{fl} &= d_{rfl} \\ p_{lim} &= p_r \\ d_{lim.cc} &= d_{r.cc} \end{aligned}$$

ELSE:

$$\begin{aligned} d_{fl} &= d_{ifl} \\ p_{lim} &= p_{im} \\ d_{lim.cc} &= d_{im.cc} \end{aligned}$$

When the implement is in front of the center of rotation, the implement can never have the limiting point, because in this setting the distance between the limiting point of the implement and the field border will always increase during turning.

When $d_{r.cc} > d_{im.cc}$, p_r needs more space during the turning and is therefore limiting.

Algorithm A-5 | Calculating the angles for the limited space FT-CPA_{cv}

$$\alpha_{p1} = \tan^{-1} \left(\frac{R + p_{lim,y}}{p_{lim,x}} \right)$$

$$d_{cc,yp1} = R + p_{lim,y} + d_{fl}$$

$$\alpha_{p2} = \sin^{-1} \left(\frac{d_{cc,yp1}}{d_{lim.cc}} \right)$$

$$d_{cc,x} = \frac{d_{cc,yp1}}{\tan(\alpha_{p2})}$$

$$\alpha_{start} = \alpha_{p2} - \alpha_{p1}$$

$$\alpha_{end} = \frac{1}{2} * \pi - \alpha_{p1}$$

Algorithm A-6 | Calculating part 2 from the limited space FT-CPA_{cv}

$$d_{cc,yp2} = \frac{p_{lim,x}}{\sin(\alpha_{hp2})}$$

$$\alpha_{lpcr} = \tan^{-1} \left(\frac{p_{lim,y}}{p_{lim,x}} \right)$$

$$d_{lpcr} = \sqrt{p_{lim,x}^2 + p_{lim,y}^2}$$

$$x_{crp2} = x_{lp}(\alpha_{hp2}) + d_{lpcr} * \cos(\alpha_{hp2} + \alpha_{lpcr})$$

$$y_{crp2} = F_2 * (d_{lpcr} * \sin(\alpha_{hp2} + \alpha_{lpcr}) - p_{lim,y} - d_{fl})$$

Algorithm A-7 | Calculate the path for a limited space FT-CPA_{cc}

Calculate the corner angle

IF $a_{int} < \pi$ THEN:

$$a_c = a_{int} + \pi$$

$$F_2 = 1$$

ELSE:

$$a_c = 3 * \pi - a_{int}$$

$$F_2 = -1$$

Calculate the center of the curve

$$x_{cc} = \frac{R}{-\tan(\frac{1}{2} * a_c)}$$

$$y_{cc} = -R$$

Use these coordinates for Equations 11-13, with the following settings:

$$\alpha_{start} = 0$$

$$\alpha_{end} = \pi - a_c$$

$$F_o = 1$$

Corrections for orientation of the corner

All y coordinates and heading directions must be multiplied with F_2

When $F_2 = -1$, a value of π must be added to the heading directions

Algorithm A-8 | Calculate the minimum turning radius for an implement at work

$$min_{eff} = 97\%$$

$$w_{eff} = min_{eff} * w_{work}$$

$$d_{crcw} = d_{cri} + d_{wa} + \frac{1}{2} * l_{work}$$

$$a = 1 - \frac{1}{min_{eff}^2}$$

$$b = w_{work} - \frac{w_{work}}{min_{eff}^2}$$

$$c = d_{crcw}^2 + \left(\frac{1}{2} - \frac{1}{4 * min_{eff}^2} - \frac{min_{eff}^2}{4} \right) * w_{work}^2$$

$$d_{ccw,y} = \frac{-b - \sqrt{b^2 - 4ac}}{2a}$$

$$R_{sw} = \sqrt{d_{ccw,y}^2 + d_{crcw}^2}$$

$$R_{work} = \sqrt{(d_{ccw,y} + w_{work})^2 + d_{crcw}^2}$$

Algorithm A-9 | Calculate the center of the curves for a C-CPA

Determine the angle of the corner:

IF clockwise working pattern:

IF $\alpha_{int} \geq \pi$:

$$\alpha_c = \alpha_{int} - \pi$$

ELSE:

$$\alpha_c = \alpha_{int} + \pi$$

ELSE:

IF $\alpha_{int} \leq \pi$:

$$\alpha_c = \pi - \alpha_{int}$$

ELSE:

$$\alpha_c = 3 * \pi - \alpha_{int}$$

$$\alpha_{oc} = 2 * \pi - \alpha_c$$

Determine α_{cC_2} :

$$\alpha_{cC_2} = \sin^{-1} \left(\frac{R_{sw} + w_{hl}}{d_{C_{32},fb}} \right)$$

Because this equation hold (sine rule):

$$\frac{\sin(\alpha_{cC_2})}{R_{sw}} = \frac{R_{sw} + w_{hl} * R_{sw}}{R_{sw} * d_{C_{32},fb}} = \frac{\sin(\frac{1}{2} * \alpha_{oc})}{d_{C_{23},fb}}$$

And this equation:

$$d_{C_{32},fb} = 2 * R_{sw} + w_{hl} - d_{C_{23},fb}$$

The following equation is determined:

$$d_{C_{23},fb} = \frac{R_{sw} * \sin\left(\frac{1}{2} * \alpha_{oc}\right) * (2 * R_{sw} + w_{hl})}{R_{sw} + w_{hl} + R_{sw} * \sin\left(\frac{1}{2} * \alpha_{oc}\right)}$$

Determine the coordinates of the center of the curves:

$$x_{C_2} = -\cos\left(\frac{1}{2} * \alpha_{oc}\right) * R_{sw}$$

$$y_{C_2} = -\sin\left(\frac{1}{2} * \alpha_{oc}\right) * R_{sw}$$

$$x_{C_1} = x_{C_2} - \cos(\alpha_{cC_2}) * (2 * R_{sw} + w_{hl})$$

$$y_{C_1} = y_{C_2} + \sin(\alpha_{cC_2}) * (2 * R_{sw} + w_{hl})$$

$$x_{C_3} = x_{C_2} + \cos(\alpha_{cC_2} - \pi + \alpha_{oc}) * (2 * R_{sw} + w_{hl})$$

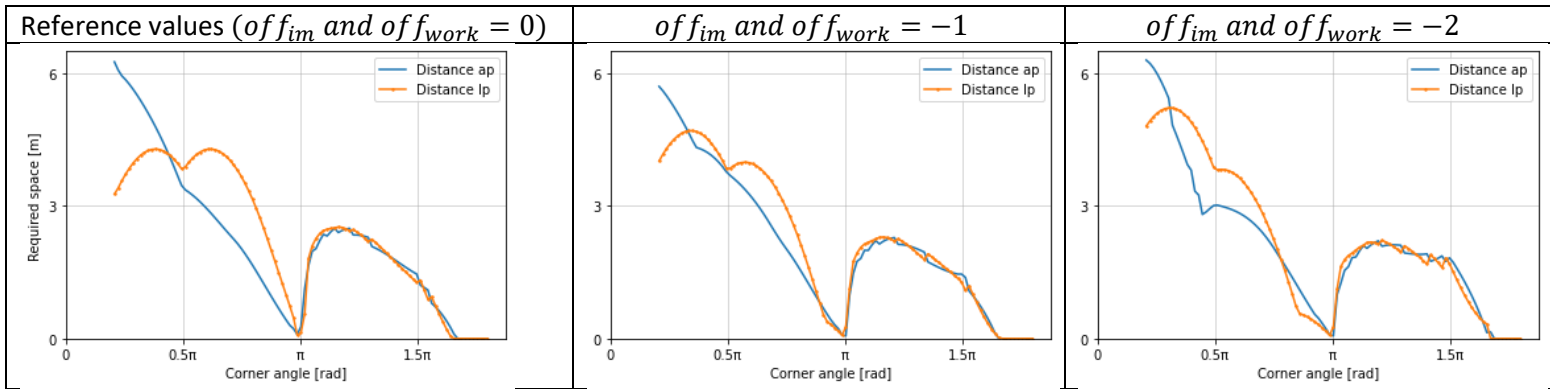
$$y_{C_3} = y_{C_2} + \sin(\alpha_{cC_2} - \pi + \alpha_{oc}) * (2 * R_{sw} + w_{hl})$$

$$x_{C_{cv}} = -\frac{R_{sw} + w_{hl}}{\tan\left(\frac{1}{2} * \alpha_c\right)}$$

$$y_{C_{cv}} = R_{sw} + w_{hl}$$

Appendix A

Varying of_{im} and of_{work} for a free space FT-CPA



Varying w_{work} and w_{im} for a free space FT-CPA

